Review

Marina Fontes de Paula Aguiar[a], Javier Bustamante Mamani[a], Taylla Klei Felix, Rafael Ferreira dos Reis, Helio Rodrigues da Silva, Leopoldo Penteado Nucci, Mariana Penteado Nucci-da-Silva and Lionel Fernel Gamarra*

Magnetic targeting with superparamagnetic iron oxide nanoparticles for *in vivo* glioma

DOI 10.1515/ntrev-2016-0101
Received September 28, 2016; accepted January 24, 2017; previously published online March 16, 2017

Abstract: The purpose of this study was to review the use of the magnetic targeting technique, characterized by magnetic driving compounds based on superparamagnetic iron oxide nanoparticles (SPIONs), as drug delivery for a specific brain locus in gliomas. We reviewed a process mediated by the application of an external static magnetic field for targeting SPIONs in gliomas. A search of PubMed, Cochrane Library, Scopus, and Web of Science databases identified 228 studies, 23 of which were selected based on inclusion criteria and predetermined exclusion criteria. The articles were analyzed by physicochemical characteristics of SPIONs used, cell types used for tumor induction, characteristics of experimental glioma models, magnetic targeting technical parameters, and analysis method of process efficiency. The study shows the highlights and importance of magnetic targeting to optimize the magnetic targeting process as a therapeutic strategy for gliomas. Regardless of the intensity of the patterned magnetic field, the time of application of the field, and nanoparticle used (commercial or synthesized), all studies showed a vast advantage in the use of magnetic targeting, either alone or in combination with other techniques, for optimized glioma therapy. Therefore, this review elucidates the preclinical and therapeutic applications of magnetic targeting in glioma, an innovative nanobiotechnological method.

Keywords: external magnetic field; glioma; iron oxide; magnetic targeting; tumor.

[a]**Marina Fontes de Paula Aguiar and Javier Bustamante Mamani:** These authors contributed equally to this work.
***Corresponding author: Lionel Fernel Gamarra,** Hospital Israelita Albert Einstein, São Paulo, Brazil; Universidade Federal de São Paulo, Unifesp, São Paulo, Brazil; and Santa Casa Misericórdia de São Paulo, São Paulo, Brazil, e-mail: lgamarra@einstein.br
Marina Fontes de Paula Aguiar and Rafael Ferreira dos Reis: Hospital Israelita Albert Einstein, São Paulo, Brazil; and Universidade Federal de São Paulo, Unifesp, São Paulo, Brazil
Javier Bustamante Mamani and Taylla Klei Felix: Hospital Israelita Albert Einstein, São Paulo, Brazil
Helio Rodrigues da Silva: Hospital Israelita Albert Einstein, São Paulo, Brazil; and Santa Casa Misericórdia de São Paulo, São Paulo, Brazil
Leopoldo Penteado Nucci: Universidade Federal de São Paulo, Unifesp, São Paulo, Brazil; and Faculdade Estácio de Sá de Goiás, Fesgo, Goiânia, Brazil
Mariana Penteado Nucci-da-Silva: LIM44, Departamento de Radiologia, USP, São Paulo, Brazil

1 Introduction

Gliomas are the most common tumors in the central nervous system [1–5]. Of these, astrocytomas, including glioblastoma multiforme (GBM), are the most prevalent and the most aggressive [3, 5, 6] representing 76% of all gliomas [7]. The classification is made in accordance with the degree of malignancy, ranging from grades I to IV. Astrocytomas types I and II are tumors that grow slowly and may be present in the brain of patients for many years without symptomatic progression, while astrocytomas types III and IV are considered the most aggressive and malignant cancers [8]. They arise from the glial cells and grow rapidly, reaching regions of the brain and spinal cord. Despite the substantial increase in basic and clinical studies over the past decades, the median survival of patients with high-grade glioma remains about a year; as a result, it is one of the most devastating and deadly of all human cancers.

The prognosis is still very limited, and current treatment involves surgery, chemotherapy and radiation therapy sessions in order to eliminate the infiltrating cells in healthy tissue [9–14]. However, unlike other cancer therapies, such as the total surgical removal of the tumor with a margin of normal tissue, this cannot be applied in brain tumors, as each brain region has a vital role.

Traditional intravenous chemotherapy has many negative effects, and low concentration of these drugs

stream through the blood-brain barrier [15–17]. The passive biodistribution used for systemic administration usually results in sub-therapeutic doses to the tumor region [18], which not only leads to elimination of the lesion but also can stimulate growth and resistance of malignant cells [19]. Another disadvantage is that chemotherapy is not selective for tumor cells, and increasing the dose may generate systemic toxicity [20]. Furthermore, because of the high molecular heterogeneity of these tumors, they remain, in most cases, refractory to treatment [21–23].

In this context, studies focused on the use of nanotechnology resource assisting the diagnosis and treatment of brain tumors are of the utmost importance. Among these, superparamagnetic iron oxide nanoparticles (SPIONs) have shown to play an important role in the diagnosis of brain tumors by magnetic resonance imaging (MRI) allowing early detection of disease, more accurate prognostic, and personalized treatments, besides the monitoring capacity and effectiveness of localized treatments [24, 25].

In a study published in 2015, Gobbo et al. [26] affirmed that the major advantage of theranostic nanomedicine in cancer treatment is the rapid evaluation of treatment results and support for therapeutic planning of patients in a personalized way.

SPIONs have magnetic properties [27], as they are composed of an iron oxide core and a polymer coating establishing important biological properties such as biocompatibility, internalization, and viability. Based on these magnetic nanoparticles, a promising approach has been widely explored using an external magnetic field of these nanoparticles for targeting to the tumor region and consequently optimize the diagnosis and/or therapy. The technique, called magnetic targeting, allows active targeting of the glioma tumor. This is a potentially interesting strategy because it is non-invasive and does not interfere with normal brain function [28].

There are two ways for nanoparticle targeting. The first is the passive targeting of nanoparticles to tumor, the cluster of nanoparticles into the microenvironment tumor due to increased permeation effect caused by increased endocytic transport, vascular exudate, and decreased lymphatic drainage [29]. However, this process does not ensure the passive intake of nanoparticles into tumor cells. Another target or driving method with nanoparticles is functional coating with specific ligand to active target in tumor cells [30]. SPION functionalization has been improved in recent years, but optimization in kinetics and biodistribution of nanoparticles are not well established for cancer treatment [30].

Therefore, other driving processes such as ultrasound [31] or magnetic field to efficient targeting of tumor have shown good results, but the efficiency of the application of the external magnetic field for SPION targeting depends on the magnetic field gradient [32]. Some clinical trials have used SPION and magnetic targeting to other tumors, but no studies have reported its use for gliomas, such as the one described in a review carried out by Lubbe et al. (2001) [33, 34].

Among the factors that may influence technical efficiency of this approach are the intensity of the applied magnetic field, the physicochemical properties of nanoparticles, cytotoxicity, their stability in the bloodstream, and the route of administration of these SPION. The magnetic targeting process is shown in Figure 1. Following the route of administration of SPION, a static external magnetic field is applied to the tumor target of these compounds; thus, this process can be monitored in real time by MRI.

Therefore, considering the importance of understanding of new approaches for the diagnosis and/or treatment of glioma, we conducted a systematic review of magnetic targeting technique. This technique is presented as a possible alternative to enhance the treatment of brain tumors using nanobiotechnology resources. This systematic review was conducted in preclinical studies as well as mimic key features of human disease, such as tumor progression kinetics and anti-tumor responses of the immune system in the presence of GBM [35, 36]. It allows the observation of the advantages and disadvantages of magnetic targeting technique.

2 Materials and methods

2.1 Search strategy

We included studies published between June 1999 and October 2016 that were found in the following databases: Cochrane Library, PubMed, SCOPUS, and Web of Science. A Boolean strategy was applied. The following sequence of keywords and Boolean operators was used: (DecS/MeSH): [(iron oxide) OR nanoparticle OR SPIO OR SPION] AND [(magnetic field) OR (magnetic targeting) OR magnetofection NOT AMF NOT (alternating magnetic field) NOT (AC magnetic field)] AND [(brain tumor) OR glioma OR glioblastoma OR gbm OR (giant cell glioblastoma) OR gliosarcoma OR astrocytoma OR (gliomatosis ependymoma) OR ependymoma OR oligodendroglioma OR oligoastrocytoma OR astroblastoma OR gangliocytoma OR ganglioma].

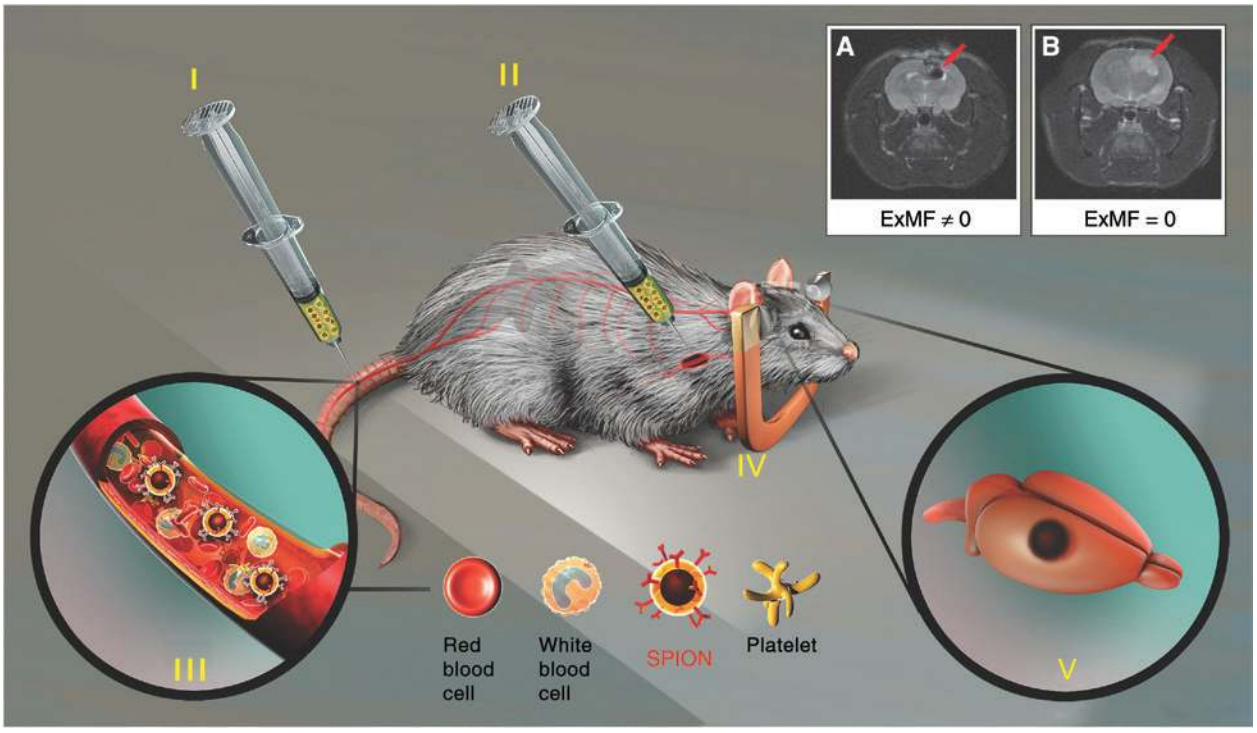

Figure 1: Representation of *in vivo* magnetic targeting using superparamagnetic iron oxide nanoparticles (SPIONs). The process begins with the SPIONs being administered caudally (I) or by carotid artery (II) and being transported by the blood flow (III). An external magnetic field (ExMF) is applied to target the tumor with SPION (IV), which are concentrated in the tumor tissue (V). MRI showing SPION accumulation (arrow) in tumor with (A) and without (B) ExMF. The illustrations are not drawn to scale.

The classification of tumors of the central nervous system, including all glial tumors, standardized by the World Health Organization [8], was sought.

2.2 Data extraction

In this review, seven of the authors independently applied the search strategy and randomly selected reports for each disease in the databases cited above.

MFA, JBM, and LFG independently searched the studies. Discrepancies in the selection of studies between the two reviewers were discussed with a third reviewer, and concensus was reached. The analysis process and table plots of this study were carried out by full consensus of coauthors, respecting the distribution above. In cases of disagreement, a third independent author resolved the differences by data addition or subtraction. Next, JBM and LFG reviewed the nanoparticle characteristics, MFA and RFR reviewed the *in vitro* characteristics, MFA, MPNS, LPN, and HRS reviewed the animal model characteristics or *in vivo* assays, and MFA, TKF, JBM, MPNS, and LFG reviewed magnetic targeting methods used to assess therapeutic efficacy. In cases of disagreement, a third independent and senior author decided by data addition or subtraction.

2.3 Selection criteria

This review included only original articles written in the English language that reported on *in vivo* magnetic targeting for SPION targeting in gliomas or on the mediation of SPION targeting on the influence of an external magnetic field. Publications indexed in more than one database (duplicate mentions), incomplete data, conference presentation, book chapters, and reports written in a language other than English, as well as studies that did not use SPION, were excluded from this review.

3 Results

After application to the search strategy, 228 original articles were identified. Of these, 23 articles were selected after exclusion of the following articles: those that appeared in more than one database; those indexed in

different databases; those with incomplete data; those appearing as a presentation at a conference, congress, or symposium; those published as book chapters; or those that did not use SPION; those that did not perform *in vivo* studies, those not containing data from the external magnetic field, or did not contain data on gliomas (Figure 2).

3.1 Physicochemical characteristics of SPION

The physicochemical characteristics of SPIONs used in selected studies are summarized in Table 1. Of the 23 selected studies, 10 studies used SPIONs synthesized in the laboratory ("in lab") [37, 38, 40–42, 45, 46, 49, 50, 55], nine used commercial SPIONs [39, 43, 44, 47, 51, 53, 57–59], and four studies looked at commercial and synthesized SPIONs [48, 52, 54, 56]. Most publications reporting on commercial SPIONs used FluidMAG [43, 47, 48, 51–53, 56–58] (Chemicell, Berlin, Germany), all used the FluidMAG-D product, only one study [51] used FluidMAG-ARA, two studies [52, 56] used FluidMAG-CMX, and one used FluidMAG-Heparin and FluidMAG-DEAE [56]. The other commercial SPIONs used were Magnetic Fluid-Amine [39], Advanced Nanotech [44], Resovist [54], and Ferrofluidics [59].

Eight studies [42, 45, 48, 49, 51, 52, 54, 56] used more than one type of SPIONs for a comparison criterion; four studies [48, 52, 54, 56] compared commercial products with synthesized *in lab*, and four studies compared only SPION synthesized [42, 45, 49, 50]. One study compared only commercial SPIONs [51]. The other studies did not compare the effect of the different SPION types and used only one type in the study, either commercial [39, 43, 44, 47, 53, 57, 58] or synthesized [37, 38, 40, 41, 46, 55]. It is noteworthy that the Pulfer study [59] compared the EMG-111 commercial nanoparticle with microspheres containing SPIONs. However, because the particle size was 1000–2000 nm, this study was not included for this review, in accordance with the previously established selection criteria.

In 14 studies [37, 38, 40–42, 45, 46, 48–50, 52, 54–56], the nanoparticles were synthesized by several chemical methods for SPION production in magnetic targeting. Among the chemical methods used were microemulsions [40], single-phase reaction (one-pot synthesis) [42, 45], hydrothermal reaction [46], sonochemical reaction [52, 55], and the coprecipitation method [49, 50, 56]. The SPION core chemical process for coating particles and conjugations with various materials to produce biocompatible particle was identified in only 14 studies [37, 38, 40–42, 45, 46, 48–50, 52, 54–56], and the crystal phase of iron oxide was identified in 12 studies [37, 38, 40, 42, 45, 48–50, 52, 54–56], 11 studies used a magnetite (Fe_3O_4), one study identified the crystalline phase as maghemite [37]; and two studies [41, 46] did not indicate which of the iron oxide crystalline phase was obtained.

The main coating material for the commercial SPIONs used was starch [43, 47, 48, 51–53, 56–58]. Other materials were dextran [39], DOX@PEG/PEI/Ps80 (doxorubicin/poly-ethylene glycol/polyethylenimine/Polysorbate 80) [38], carboxymethyldextran (CMD) [52, 56], carboxydextran [54], heparin, and dextran-diethylaminoethyl [56]. Among the studies summarizing the SPIONs used, the coating materials included DNPH (starch cross-linked, aminated, poly(ethylene glycol) (PEG)ylated and heparin-conjugated magnetic nanoparticles) [42], BCNU (1,3-bis(2-chloroethyl)-1-nitrosourea) [45], Dextrana-Fluorophore-arginine-glycine-aspartate (Dx-F-RGD) [46], SPAnNa-BCNU (poly[aniline-co-sodium *N*-(1-one-butyric-acid) aniline]-BCNU) [49], SPAnH(poly-[aniline-co-N-(1-one-butyric acid) aniline]) [50], SPAnH-epirubicin [54], and gum arabic [56]. One study [37] used SPION complex to make rhodamine-labeled magnetic fluid-loaded PEGylated liposome (MFL) nanoparticle. Some studies have analyzed commercial SPIONs [43, 44, 51, 59] or involved synthesized SPIONs that used a combination of materials to form biocompatible coverage. Fan [39] used commercial SPION coating with dextran to develop SPIO-doxorubicin-conjugated microbubbles. Pulfer [59] used dextran particles with aminodextran and coverage, but as mentioned above, these are treated microspheres and were not considered in this review.

The physicochemical characteristics of the commercial SPIONs used were (I) Magnetic Fluid-Amine (MagQu Co Ltd, New Taipei City, Taiwan) with a magnetite core, average hydrodynamic size of 35.7 nm, coated with dextran, and provided at an iron concentration of 8.12 mg/ml; (II) Fl1uidMAG-d (Chemicell®, Berlin, Germany) with a magnetite core, average core diameter of 12 nm, average hydrodynamic size of 50–251 nm, coated with starch, and provided at an iron concentration of 25 mg/ml; (III) FluidMAG-CMX (Chemicell®, Berlin, Germany) with a magnetite core, an average hydrodynamic diameter of 100 nm, covered with carboxymethyldextran, and provided at an iron concentration of 25 mg/ml; (IV) FluidMAG-ARA (Chemicell®, Berlin, Germany) with a magnetite core, average core diameter of 10 nm and 225 nm average hydrodynamic size, covered and provided with glucuronic acid at an iron concentration of 25 mg/ml; (V) Heparin-FluidMAG (Chemicell®, Berlin, Germany) with a magnetite core, average hydrodynamic size of 100 nm, coated

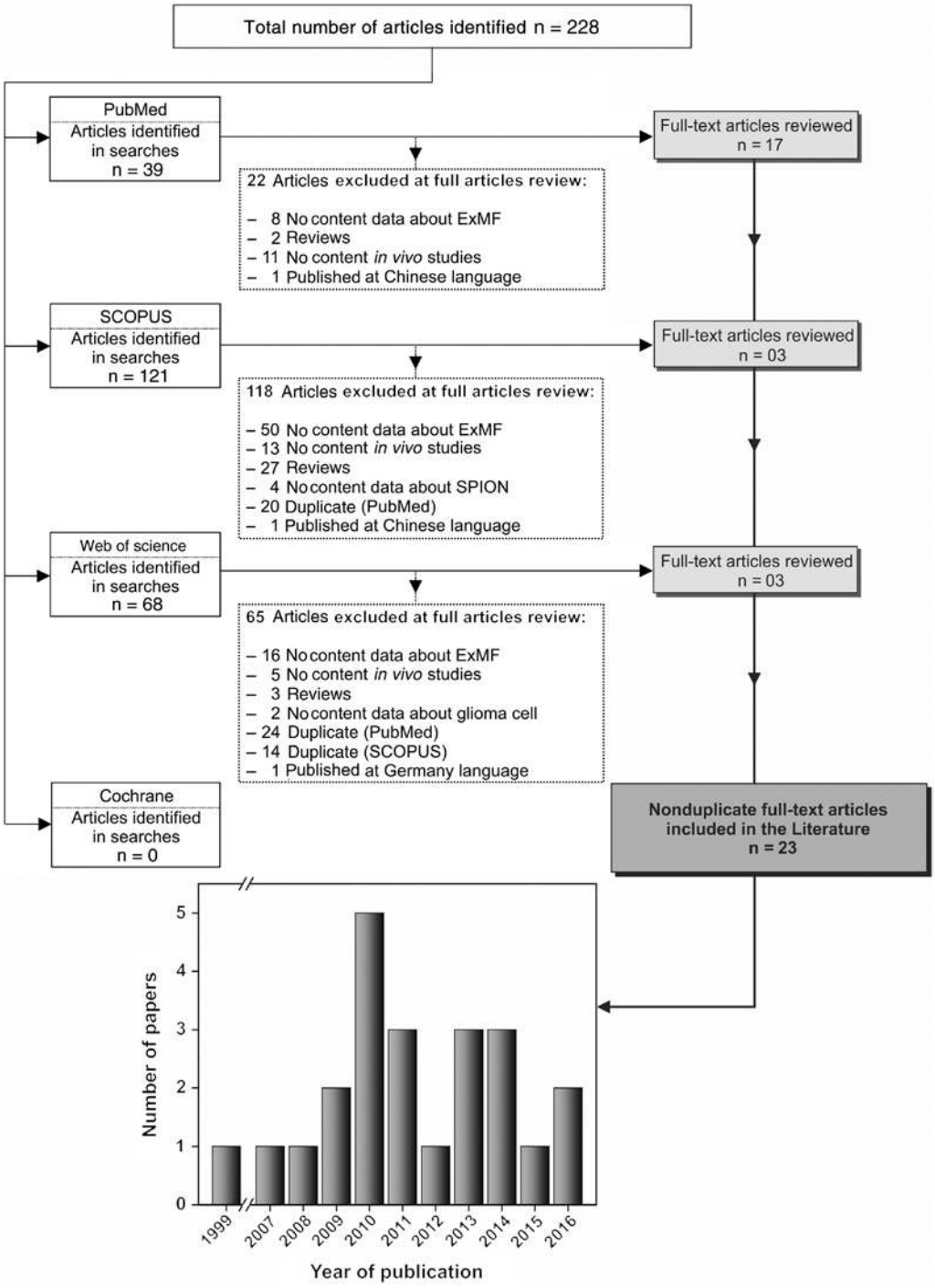

Figure 2: Flowchart of selection process of studies included in the review.

with heparin, and provided at an iron concentration of 10 mg/ml; (VI) FluidMAG DEAE (Chemicell®, Berlin, Germany) with a magnetite core, average hydrodynamic size of 100 nm, coated with diethylaminoethyl-dextran, and provided at an iron concentration of 25 mg/ml; (VII) Resovist® (Bayer Schering Pharma AG, Berlin, Germany), which are nanoparticles of a crystalline phase mixture of magnetite and magnetite, average core diameter of 5.9 nm and 63.8 nm average hydrodynamic size, coated with carboxydextran, and provided at an iron concentration of 27.9 mg/ml; (VIII) Advanced Nanotech (Taiwan), with a core diameter of 6–10 nm and 700–4000 nm hydrodynamic size, and provided at an iron concentration of 0.68 mg/ml; (IX) EMG-111 (Ferrofluidics, Corp. Nashua,

Table 1: Physicochemical characteristics of SPION used in the magnetic targeting process.

Refs.	Iron oxide	(Fe) (mg/ml)	Core/hydrodynamic size (nm)	Coating	Ms (Emu/g Fe)	R_2 relaxivity (s^{-1} мм$^{-1}$)	Tb (K)	ζ potential (mV)	Manufacture
[37]	Fe_3O_4	8.12	NA/35.7	Dextran[SDMB]	NA	NA	NA	NA	Magnetic Fluid-Amine[a]
[38]	Fe_3O_4	NA	11.5/28.7	PEG/PEI/Ps 80	47.3	88.56	NA	19	Synthesized
			12.3/58	DOX@PEG/PEI/Ps 80	24.1	NA	NA	28	
[39]	γ-Fe_2O_3	NA	8/13	[a][i]		0.259	NA	NA	Synthesized
[40]	Fe_3O_4	NA	5/100–150	Lf-MDCs	NA	NA	NA	NA	Synthesized
[41]	NA	50	267.3	S-PEG-βglu	NA	NA	NA	− 4.3	Synthesized
[42]	Fe_3O_4	2.4	NA/164.9	DNPH 1	64.43	NA	NA	− 29.1	
		2.4	NA/166.6	DNPH 2	65.42			− 20.3	
		2.4	NA/162.2	DNPH 3	62.87			− 8.9	Synthesized
		2.4	NA/171.4	DNPH 4	66.59			− 3.6	
[43]	Fe_3O_4	40	12/251	βglu-s-IO	60	118.3	NA	+18.5	G100 (FluidMAG-D)[b]
[44]	NA	0.68	6–10/700–4000	Dox-SPIO	0.014	107.3	NA	NA	Advanced Nanotech (Taiwan)
[45]	Fe_3O_4	14.1	5/215–230		NA	164			
		18.8	5/NA	BCNU	57	183	NA	NA	Synthesized
		28.2	5/180–205		NA	208			
[46]	NA	NA	8/97	Dx-F-RGD	NA	NA	NA	NA	Synthesized
[47]	Fe_3O_4	25	12/110	Starch	94	43.8	160	− 12	G100 (FluidMAG-D)[b]
[48]	Fe_3O_4	75	12/104	Starch	98.6	43.8	160	− 12	G100 (FluidMAG-D)[b]
			12/142	Starch-PEG (5 kDa)	103.1	NA	NA	+24.4	Synthesized
			12/168	Starch-PEG (20 kDa)	104.2	NA	NA	+25.6	Synthesized
[49]	Fe_3O_4	NA	NA/89	SPAnNa-BCNU (9.6%)	62.5	NA	NA	− 19.6	Synthesized
				SPAnNa-BCNU (19.7%)	37.6			− 33.1	
				SPAnNa-BCNU (14.4%)	55.9			− 35.1	
[50]	Fe_3O_4	NA	NA/10–20	–	66.2	NA	NA	NA	Synthesized
				SPAnH	37.6				
[51]	Fe_3O_4	25	12/110	Starch	125	43.8	NA	− 12	G100 (FluidMAG-D)[b]
		NA	10/225	GPEI	93	NA	NA	37.2	Gara (FluidMAG-ARA)[b]
[52]	Fe_3O_4	25	NA/100	CMD	94	NA	NA	NA	FluidMAG-CMX[b]
		25	NA/100	Starch	94	43.8	160	− 12	FluidMAG-D[b]
		0.7	9/40–280	CMD	69.4	NA	NA	− 19.4	Synthesized
[53]	Fe_3O_4	25	12/110	Starch	94	43.8	160	− 12	G100 (FluidMAG-D)[b]
[54]	Fe_3O_4- γ-Fe_2O_3	27.9	5.9/63.8	Carboxydextran	73.7	98.4	NA	45	Resovist®[c]
	Fe_3O_4	NA	10.9/73.7	SPAnH-epirubicin	51.8	30.0	NA	NA	Synthesized
			11.4/75.8		65.9	102.3			
			12.3/83.4		81.7	185.0			
[55]	Fe_3O_4	NA	8.4/NA	CMD	NA	NA	NA	NA	Synthesized
[56]	Fe_3O_4	25	NA/100	CMD	94				FluidMAG-CMX[b]
	Fe_3O_4	10	NA/100	Heparin	94	NA	NA	NA	FluidMAG-Heparin[b]

Table 1 (continued)

Refs.	Iron oxide	(Fe) (mg/ml)	Core/hydrodynamic size (nm)	Coating	Ms (Emu/g Fe)	R_2 relaxivity (s^{-1} мм$^{-1}$)	Tb (K)	ζ potential (mV)	Manufacture
	Fe_3O_4	25	NA/100	Dextran-diethylaminoethyl	94				FluidMAG-DEAE[b]
	Fe_3O_4	25	12/110	Starch	94	43.8	160	– 12	G100 (FluidMAG-D)[b]
	Fe_3O_4	10	14/118	Gum arabic	93.1	NA	NA	NA	Synthesized
[57]	Fe_3O_4	25	12/110	Starch	94	43	160	– 12	G100 (FluidMAG-D)[c]
[58]	Fe_3O_4	25	12/110	Starch	94	43.8	160	– 12	G100 (FluidMAG-D)[b]
[59]	Fe_3O_4	NA	NA/1000–2000	Aminodextran					NA
			NA/1000–2000	Dextran	NA	NA	NA	NA	NA
			10/20	NA					EMG-111[d]

SPIO, superparamagnetic iron oxide; Fe, ferro; Ms, saturated magnetization strength; R2, relaxivity transversal; Tb, blocking temperature; Lf-MDCs, lactoferrin-tethered magnetic double emulsion nanocapsules; PEG, poly(ethylene glycol); S-PEG-βglu, starch cross-linked, aminated, PEG modification, conjugation of β-glucosidase; DNPH, starch cross-linked, aminated, PEGylated and heparin-conjugated MNP; βglu-s-IO, β-glucosidase to aminated, starch-coated, iron oxide; DOX, doxorubicin; Dox-SPIO, doxorubicin-SPIO-circulating microbubbles; BCNU, (1,3-bis(2-chloroethyl)-1-nitrosourea)-loaded nanobubbles; Dx-F-RGD, Dextrana-Fluorophore- arginine-glycine-aspartate; S-PEG, starch cross-linked, aminated, and modified with PEG; SPAnNa-BCNU (9.6%), poly[aniline-co-sodium N-(1-one-butyric acid) aniline] + BCNU: 9.6% (w/w) SPAnNa; SPAnH, (poly-[aniline-co-N-(1-one-butyric acid) aniline]); PEI, polyethylenimine; GPEI, PEI-modified magnetic nanoparticles coated with gum arabic polysaccharide; CMD, carboxymethyl-dextran; Ps 80, Polysorbate 80; NA, not identified; SDMB, SPIO-doxorubicin-conjugated microbubbles.

[a]MagQu Co Ltd (New Taipei city, Taiwan).

[a]Rhodamine-labeled magnetic-fluid-loaded PEG-ylated liposomes (MFLs).

[b]Chemicell® (Berlim, Germany).

[c](Bayer Schering Pharma AG, Berlin, Germany).

[d]Ferrofluid (EMG-111, Ferrofluidics Corp, Nashua, NH, USA).

NH, USA) with an average core diameter of 10 nm and 20 nm average hydrodynamic size.

3.2 Characteristics of cells used for tumor induction

The characteristics of cells used for tumor induction for further *in vivo* studies are summarized in Table 2. Most of the selected studies used glial cells of origin [41–44, 46–58], with only four studies [37, 40, 45, 59] specifically using cells that originated from a glioblastoma rat, called RG21. Among all the studies, only that by Fu [46] and Marie [37] used human cells, designated U87MG, and capable of originating a grade IV astrocytoma or glioblastoma. All other studies used cells from *Rattus norvegicus* [38–45, 47–59] species. Of these, the most widely used cell line was 9L, identified in 11 studies [41–43, 47, 48, 51–53, 56–58].

The 9L cells originate the gliosarcoma tumor (more aggressive) in rats, mimicking important characteristics of human tumors, such as the pattern of tumor growth, growth factor expression, and metastasis. Another cell line widely used was the C6 (more solid and circumscribed with rat tumor), reported in seven studies [38, 39, 44, 49, 50, 54, 55]. These cells were cloned rat glioma induced by N-nitrosomethylurea [60] and have been widely used for a variety of studies on tumor growth, invasion, migration, neovascularization, growth factor regulation, and biochemical studies because they are morphologically very similar to glioblastoma multiforme [61, 62].

3.3 *In vivo* experimental model of glioma

The experimental model characteristics, as well as tumor induction parameters, are described in Table 3. All studies selected for this review are in preclinical testing and have used experimental models of rats or mice and clinical trials that have been performed. The small number of clinical studies on this subject shows that progress is early, and more work is needed on the nanobiotechnological tools for the diagnosis and treatment of gliomas.

Among the rodents identified, seven studies used mice [37, 40–43, 45, 46], 17 used rats in their experiments [38, 39, 44, 45, 47–59], and Huang used both rats and mice [45]. From the studies that were based on rat models, the

Table 2: Cell characteristics of tumor induction.

Refs.	Tumor cell line	Cell type	Organism	Tumor type	Medium culture
[37]	C6	Glial Cell	Rat/RN	Glioma	DMEM/F_{12}; 10% FBS; 1% Pen Strep; 1.2 g $NaHCO_3$
[38]	C6	Glial Cell	Rat/RN	Glioma	H-DMEM; 10% FBS
[39]	U87MG	Glial cell	Human	Glioblastoma	DMEM; 10% FBS; 1% Pen Strep Amp-B
[40]	RG2	Glioblastoma	Rat/RN	Differentiated malignant glioma	DMEM; 10% FBS; 1% Pen Strep
[41]	9L	Glial cell	Rat/RN	Gliosarcoma	DMEM; 10% FBS; 100 IU/ml Pen; 100 mg/ml Strep
[42]	9L	Glial cell	Rat/RN	Gliosarcoma	DMEM; 10% FBS; 1% Pen Strep
[43]	9L	Glial cell	Rat/RN	Gliosarcoma	DMEM; 10% FBS; 100 IU/ml Pen; 100 mg/ml Strep; 0.29 mg L-glut
[44]	C6	Glial cell	Rat/RN	Glioma	DMEM/F_{12}; 10% FBS; 1% Pen Strep
[45]	RG2	Glioblastoma	Rat/RN	Differentiated malignant glioma	RPMI 1640/FCS
[46]	U87MG	Glial cell	Human	Glioblastoma, Astrocytoma	NA
[47]	9L	Glial cell	Rat/RN	Gliosarcoma	NA
[48]	9L	Glial cell	Rat/RN	Gliosarcoma	DMEM; 10% FBS; 1% antibiotics; 0.29 mg L-glut
[49]	C6	Glial cell	Rat/RN	Glioma	MEM; 10% FBS; 1% Pen Strep
[50]	C6	Glial cell	Rat/RN	Glioma	MEM; 10% FBS; 1% Pen Strep
[51]	9L	Glial cell	Rat/RN	Gliosarcoma	DMEM; 10% FBS; 100 IU/ml Pen; 100 µg/ml Strep; 0.29 mg L-glut
[52]	9L	Glial cell	Rat/RN	Gliosarcoma	DMEM; 10% FBS; 100 IU/ml Pen; 100 µg/ml Strep; 0.29 mg L-glut
[53]	9L	Glial cell	Rat/RN	Gliosarcoma	DMEM; 10% FBS; 100 IU/ml Pen; 100 µg/ml Strep; 0.29 mg L-glut
[54]	C6	Glial cell	Rat/RN	Glioma	NA
[55]	C6	Glial cell	Rat/RN	Glioma	MEM; 10% FBS; 1% Pen Strep
[56]	9L	Glial cell	Rat/RN	Gliosarcoma	DMEM; 10% FBS; 100 IU/ml Pen; 100 µg/ml Strep; 0.29 mg L-glut
[57]	9L	Glial cell	Rat/RN	Gliosarcoma	DMEM; 10% FBS; 100 IU/ml Pen; 100 µg/ml Strep; 0.29 mg L-glut
[58]	9L	Glial cell	Rat/RN	Gliosarcoma	DMEM; 10% FBS; 100 IU/ml Pen; 100 µg/ml Strep; 0.29 mg L-glut
[59]	RG2	Glioblastoma	Rat/RN	Differentiated malignant glioma	DMEM; 10% FBS

DMEM, Dulbecco's modified Eagle's medium; DMEM/F_{12}, DMEM containing growth fator F_{12}; H-DMEM, DMEM, high glucose; MEM, minimum essential medium; EMEM, Eagle's minimum essential médium; FBS, fetal bovine serum; Pen Strep, penicillin streptomycin; Amp-B, amphotericin B; L-glut, L-glutamine; FCS, fetal calf serum; RN, *Rattus norvegicus*; NA, not identified.

Table 3: Experimental design of glioma *in vivo* study.

Refs.	Animal description				Tumor induction						
	Animal	Sex	Age/weight (week/g)	T/NG	Cell type	Cell number	AV (µl)	Vehicle	AT (min)	Localization	Coordinates (D; A; L/mm)
[37]	Sprague-Dawley	Male	NA/20–25	16/4	C6	7×10^5	7	PBS	10	Str	4.5; 0.5; 3
[38]	Sprague-Dawley	Male	NA/25–35	48/12	C6	1×10^6	10	PBS	10	RH	5.0; NA; 3
[39]	Swiss nude mice	Female	8/21–27	12/6	U87MG	5×10^4	5	NA	NA	Str (RH)	3; 0.5; 2
[40]	BALB/c nude mice	Female	3–5/NA	15/3	RG2	5×10^7	50	PBS	NA	SC (Lf and Rf)	NA
[41]	Black C57BL6 mice	NA	NA/20–25	NA	9L	2×10^6	50	Serum-free DMEM	NA	SC (Rf)	NA
[42]	Nude mice	Male	NA/18–22	NA	9L	10^9	100	Serum-free DMEM	NA	SC (Lf)	NA
[43]	Nude mice	NA	NA	NA	9L	2×10^6	50	Serum-free DMEM	NA	SC (Rf)	NA
[44]	Rat/SD	Male	NA/200–250	43/NA	C6	2.5×10^3	5	NA	10	NA	4.5; 0.5; 3
[45]	Rat/Wistar	NA	NA/NA	48/24	RG	10^4–10^5	100	Saline	NA	SC (right leg)	NA
	Nude mice	Female	24/NA	20/5	2					SC	
[46]	SCID mouse	Male	NA/28	NA	U87 MG	2×10^7	20	NA	NA	SC	NA
[47]	Rat/Fisher344	Male	NA/125–150	NA	9L	10^6	10	Serum-free DMEM	NA	RF	3; NA; NA
[48]	Rat/Fisher344	Male	NA/125–150	NA/4–5	9L	10^5	10	Serum-free DMEM	NA	RF	3–4; 1; 5
[49]	Rat/SD	Male	14–18/250–300	24/6	C6	5×10^5	5	MEM	10	Str	4.5; 0.5; 3
[50]	Rat/SD	Male	14–18/320–350	64/3–6 or 14	C6	5×10^5	5	MEM	10	Str	4.5; 0.5; 3
[51]	Rat/Fisher344	Male	NA/125–150	NA	9L	10^6	10	Serum-free DMEM	NA	RF	3; NA; NA
[52]	Rat/Fisher344	Male	NA/150	NA	9L	10^6	10	Serum-free DMEM	10	RF	3; 1; 5
[53]	Rat/Fisher344	Male	NA/125–150	NA/5–8	9L	10^6	10	Serum-free DMEM	NA	RF	3; 1; 5
[54]	Rat/SD	NA	NA/300–400	14/NA	C6	10^6	NA	NA	NA	NA	NA
[55]	Rat/SD	Male	14–18/350	NA	C6	5×10^5	5	MEM	10	Str	4.5; 0.5; 3
[56]	Rat/Fisher344	NA	NA/200	NA/3–4	9L	10^5	10	Serum-free DMEM	NA	RF	3–4; NA; NA
[57]	Rat/Fisher344	Male	NA/125–150	NA/6	9L	10^6	10	Serum-free DMEM	10	RF	3; 1; 5
[58]	Rat/Fisher344	Male	NA/125–150	NA/6	9L	10^6	10	Serum-free DMEM	10	RF	3; NA; NA
[59]	Rat/Fisher344	Male	NA/225/250	NA/3	RG2	2×10^3	2	DMEM	0.5	RF	4.5; NA[a]; 2

SD, Sprague Dawley; T, total number of animals; NG, number of animals/group; AT, administration time, AV, administration volume; SC, subcutaneously; Lf, left flank; Rf, right flank; RF, right forebrain; RH, right Hemisphere; Str, striatum; D, depth; A, anterior from the bregma; L, lateral from the bregma; DMEM, Dulbecco's modified Eagle's medium; MEM, minimum essential medium; PBS, phosphate-buffered saline; NA, not identified.

most commonly used species was Fisher 344, identified in nine studies [47, 48, 51–53, 56–59]. The second most used species were the Sprague-Dawley rats, reported in seven studies [38, 39, 44, 49, 50, 54, 55]. Only one study [45] used Wistar rats. With regard to studies that used mice, the main species was nude mice, identified in four studies [37, 40, 42, 43]. Only one study [46] used SCID mice, and another study [41] used BLACK C57BL6 species.

The weights of the animals used in the various studies varied widely. For studies that used Fisher 344 rats, the weights ranged from 125 to 150 g in seven studies [47, 48, 51–53, 57, 58], 200 g in the study by Zhang [56], and ranged from 225 to 250 g in the study by Pulfer [59]. Among the studies that used male Sprague-Dawley rats, the weights varied between 200 and 250 g in Fan's study [44], 250 and 300 g in Hua's study [49], 320 and 350 g in the study by Chen [50], and 300 and 400 g in other studies [54, 55]. Huang [45] used Wistar rats and mice, both nude, in his study but did not provide the selected weight. Of the other three studies that used nude mice, the weight ranged from 18 to 22 g in Zhang's study [42] but was not reported in the studies of Fang [40] and Zhou [43]. Only one study [41] that used C57BL6 black mice selected animals weighing 20–25 g, and Fu [46], the only study using SCID mice, considered animals weighing 28 g.

Regarding the sex of the rodents used, three studies [37, 40, 45] used females, while most selected male rats or mice [38, 39, 42, 44, 46–53, 55, 57–59] and four studies [41, 43, 54, 56] did not provide this information. A few studies have reported the total number of animals and number of animals used per group. Among the studies that did provide this information, the variability was wide, ranging from three to eight animals per group [38–40, 45, 48–50, 53, 56–59].

The choice of animal model is often directly related to the selected cell line. Thus, most studies that have opted for cell line 9L inoculated these cells in Fisher 344 rats [47, 48, 51–53, 56–58]. However, two studies inoculated 9L cells in nude mice [42, 43], and one study did so in black C57BL6 mice [41]. However, the study by Pulfer [59] used the cell line RG2 in Fisher 344 rats, unlike Fang [40] and Huang [45], who used this same lineage but in BALB/c nude mice and Wistar rats, respectively. All authors who used the C6 cell line chose the Sprague-Dawley [38, 39, 44, 49, 50, 54, 55] species. The only study that used a human cell line (RG2) inoculated these cells in SCID mice [46], which are useful as models for the lack of immunity of B and T cells and, hence, are susceptible to human disease in a chronic state.

The number of inoculated cells for tumor induction also differed in relation to both the cell chosen as the site of the tumor and the species used. Studies induced subcutaneous tumor inoculated [40–47], in general, proportionally inoculated more cells. Among the studies that implanted tumor cells in the mouse flank, two used 2×10^6 9L cells [41, 43], two studies used 5×10^7 and 10^4–10^5 RG2 cells [40, 45], one inoculated 10^9 9L cells [42], one study used 2×10^7 U87MG cells [46]. Another site frequently used for tumor induction was the right cerebral hemisphere, identified in 11 studies [37, 39, 47, 48, 51–53, 56–59]. In this place of glioma induction, the studies that used rats as an experimental model inoculated 10^6 9L cells [47, 51–53, 57, 58], 10^5 9L cells [46, 56], and 2×10^3 RG2 cells [59]. The striatum was also used as a place of tumor induction and was chosen only for the rat model whose tumors were induced between 10^4 and 10^6 C6 cells [37–39, 49, 50, 55]. Fan [44] inoculated 2.5×10^3 9L cells but did not report the site of induction. Liu [42] also did not provide the site of tumor induction but reported the use of 10^6 C6 cells to induce the tumor. Therefore, the major model used in the selected studies was lineage 10^6 9L cells inoculated into the right cerebral hemisphere (striatum) of male Fisher 344 rats weighing 125–150 g.

The vehicle suspension for inoculation of the tumor cells in animals was mostly DMEM fetal bovine serum free, identified in 11 studies [41–43, 47, 48, 51–53, 56–58]. Pulfer's study [59] also used DMEM as a vehicle but did not specify whether it was fetal bovine serum free. Other vehicle suspensions were PBS [38–40] and saline [45] and MEM [49, 50, 55], while three studies [44, 46, 54] did not report the vehicle of choice. A few studies reported the duration of administration of the cells to the tumor site. When mentioned, the duration was 10 min in nine studies [38, 39, 44, 49, 50, 52, 55, 57, 58] and 30 s in one study [59].

The coordinates used for tumor induction also varied among the studies. In studies that inoculated cells subcutaneously, this information does not apply; however, the studies that induced glioma into the right hemisphere of the brain or into the striatum region were based on depth coordinates that were latero-lateral and anterior-posterior in relation to the stereotactic atlas. The average depth was 4.5 mm in five studies [44, 49, 50, 55, 59] and 3 mm in the other 10 studies [38, 39, 47, 48, 51–53, 56–58]. Only Liu [54] and Marie [39] did not report the depth used for inoculation of the tumor cells. In relation to the anteroposterior coordinate (axis), some studies reported that the cells were inoculated in the right hemisphere at 1 mm anterior to the bregma [48, 52, 53, 57] or 2 mm posterior to the bregma [59]; others did not provide this information [47, 51, 56, 58]. The latero-lateral coordinate used in the studies that deployed the cells in the right hemisphere was 5 mm [48, 52, 53, 57], 2 mm [59], or not reported

[47, 51, 56, 58]. Among the studies [37–39, 49, 50, 55] whose administration of the cells was into the striatum site, the anteroposterior coordinate was 0.5 mm and 3 mm latero-lateral in relation to the bregma.

3.4 Experimental design of magnetic targeting

The parameters of the transfection process mediated by nanoparticles, also called magnetic targeting, are described in Table 4. For this review, we selected studies that performed magnetic targeting by imposing an external static magnetic field for more efficient and specific targeting of SPION at the tumor region.

The magnetic targeting process consists in SPION systemic injection for later magnetic targeting. Most studies administered SPIONs on the 10th day after tumor induction [44, 46, 47, 49, 51–58] (described in Table 3). Two other studies administered SPIONs 7–14 days after tumor induction [40, 45]. Pulfer's study [59] performed the procedure 14–21 days after induction. The other studies [41–43] did not specify this information. However, the appropriate day to perform magnetic targeting process was reported as that on which the tumor volume (mm^3) is 300–400 [41], 300–500 [42], or 100–200 [43]. Even among articles that determine the day of SPION administration in animals, most take into account tumor volume [40, 44, 47, 48, 51–53, 57, 58].

The concentration of the nanoparticles (mg Fe/kg body weight) administered in the studies varied. The concentration used most often was 12 mg Fe/kg [41, 43, 45, 47, 48, 51, 52, 56–58]. Hua [49] used a concentration of 10.5 mg Fe/kg and Huang [55] used 10 mg Fe/kg, while Pulfer [59] administered nanoparticles at a concentration of 4 mg Fe/kg. Zhang [42], Chen [50], and Chertok [53] used different concentrations of nanoparticles ranging from 4 to 20 mg Fe/kg, 0.5 to 8 mg Fe/kg, and 12 to 25 mg Fe/kg, respectively. Marie's [37] study had the highest concentration of iron (29 mg Fe/kg). The other studies [40, 44, 46, 54] did not report this information. Regarding the suspension vehicle used to administer the SPION in different routes, most of the studies reporting this information used saline [39, 40, 44, 50] or PBS [37, 38, 47, 48, 51, 53, 56–58]; Pulfer [59] used Tween 80/saline suspension as a vehicle. The most frequent administration route was intravenously, identified in 17 studies [37–43, 45–48, 51–53, 56–58]. Other studies administered nanoparticles via the jugular vein [44, 49, 50, 54, 55] or carotid artery [47, 51, 59]. Of these, Chertok [47, 51] used tail injection and carotid administration in order to compare the efficiency of magnetic targeting process performed in different routes. Only three studies reported the duration of nanoparticle infusion: 10 min in two studies [57, 58] and 2 min in the study by Pulfer [59]. The main route of administration of SPIONs in selected studies was tail vein, with 12 mg Fe/kg in PBS vehicle.

As is known about the *in vivo* magneto targeting process, all studies used an external and static magnetic field with different characteristics for directing nanoparticles to the tumor region. Regarding the intensity of the field used, four studies [40, 46, 48, 54] used a magnetic field of 0.2 T, nine studies [38, 41–43, 47, 49, 51, 55] used a magnetic field of 0.3–0.35 T, and five studies [37, 39, 52, 53, 57, 58] used only 0.4–0.5 T. The highest intensity values found were 0.6 T [59] and 1.18 T [45]. Chertok [47] and Liu [54] used different field strengths to promote magnetic targeting: from 0.15 to 0.35 T and from 0.2 to 0.55 T, respectively. Only two studies [44, 56] did not report the intensity of the external magnetic field used. The duration of application of the magnetic field in each study also varied: 0.25–1.5 h [42], 0.08–48 h [45], 0.16–2 h [46], 3–24 h [54], and 2–24 h [55]. Most other studies applied the magnetic field for only 30 min [47, 51–53, 56–59], four studies [38, 41, 43, 48] applied it for 1 h, Fang [40] did so for 6 h, and Hua [49] and Chen [50] did so for over 24 h. External and static magneto were used in most studies, by using a magnetic field of 0.3 T and 30 min duration.

To optimize the efficiency of the magnetic field, many studies used adaptations to the field for better targeting. Seven studies [44, 52, 53, 56–59] did not complement the magnet with any artifice. Among the adjustments used, Fang [40] affixed the magnet to the animal's head using a bandage, Zhou [41, 43] used a cylindrical neodymium magnet connected to the main magnet, Zhang [42] linked one small cylindrical magnet 6.4 mm in diameter to the other third cylindrical neodymium magnet 51 mm in diameter, Huang [45] used a directed magnetic field 1 cm in diameter, Fu [46] chose a rectangular neodymium magnet with dimensions of $22 \times 7.5 \times 7.5\ mm^3$, Chertok [47, 51] used an electromagnet coupled to a cylindrical neodymium magnet 9 mm in diameter, Cole [48] used a cylindrical neodymium magnet 9 mm in diameter secured to a pole 40 mm in diameter, Hua [49], Chen [50], and Huang [55] set the magnet in the skull of rats, and Liu [42] attached the magnet to the animals' scalp and secured it with a plastic band.

The main applications of the magnetic targeting process identified by the studies in question were magnetically targeted drug delivery [40, 41, 43, 47–49, 51, 52, 55–59], a new platform for monitoring magnetic resonance and targeted drug delivery [42], increased therapeutic efficacy of chemotherapeutic agents [44], development of a nanobubble system for cancer treatment [45], early cancer

Table 4: Experimental design of magnetic targeting.

Refs.	Nanoparticle administration							Magnetic field			
	Days after induction	Tumor size (mm^3)	Nanoparticle	Dose (mg/kg)	Vehicle	RA	AT (min)	MF (T)	Time of field (h)	Magnet	Application
[37]	10	22.9	SD-MB	20	Saline	Jugular vein	NA	0.48	3	Placed tightly to the scalp of the animal's left head	Targeted drug delivery
[38]	14	~7.5	PEG/PEI/Ps 80-MP DOX@PEG/PEI/Ps 80-MP	2; 6	PBS	Tail vein	NA	0.3	1	NdFeB disk (2 cm D)	Theranostic treatment
[39]	14	4.3	MFLs	29.8	PBS	Tail vein	NA	0.4	4	NdFeB (8 mm D, 4 mm height)	Targeting of malignant brain tumors
[40]	7–14	50–100	Lf-MDCs-MP; Lf-Cur-MDCS-MP; Lf-Dox-MDCs-MP; Lf-Dox/Cur-MDCs-MP	NA	Saline	Tail vein	NA	0.2	6	Wrapped using a bandage	Targeted drug delivery
[41]	NA	300–400	S-PEG-β-Glu-MP	12	NA	Tail vein	NA	0.32	1	NdFeB cylindrical on 3 tandem DYOYO-52	Targeted drug delivery
[42]	NA	300–500	DNPH 3-MP	4; 8; 12; 16; 20	NA	Tail vein	NA	0.32	0.25; 0.5; 0.75; 1l 1.5	3 DYOYO-N52 cylindrical (51 mm D) + 1 D48-N52 cylindrical (6.4 mm D)	Novel nano-platform for MRI and MT
[43]	NA	100–200	β-Glu-S-MP	12	NA	Tail vein	NA	0.32	1	NdFeB cylindrical (9 mm D) on 3 tandem DYOYO-52	Targeted drug delivery
[44]	10	19.50 ± 9.92	DOX-SPIO-MP	NA	Saline	Jugular vein	NA	NA	0.16	NA	Improving therapeutic efficacy of chemo agents
[45]	7, 10, or 14	NA	BCNU-MP	12	NA	Tail vein	NA	1.18	0.08; 0.5; 3; 6; 12; 24; 48	Focused MF (1 cm D)	Nanobubble system as a cancer therapy
[46]	10	NA	Dx-F-RGD -MP	NA	NA	Tail vein	NA	0.2	0.16; 0.2; 2	NdFeB N52 rectangular bar ($7.5 \times 7.5 \times 22$ mm^3)	Early cancer detection and targeted therapy
[47]	10	70–90	Starch-MP	12	PBS	Tail vein; carotid artery	NA	0.15; 0.35	0.5	Dipole electromagnet + cylindrical NdFeB (9 mm D)	Targeted drug delivery
[48]	11	50–100	Starch-MP; Starch-PEG (5 kDa)-MP; Starch-PEG (20 kDa)-MP	12	PBS	Tail vein	NA	0.2	1	Cylindrical NdFeB (9 mm D) secured to a 40 mm D pole	Targeted drug delivery
[49]	10	NA	SPAnNa-BCNU-MP	10.5	NA	Jugular vein	NA	0.3	> 24	NdFeB fixed to the cranium of rats	Targeted drug delivery
[50]	17	NA	SPAnH-MP	0.5; 1; 5; 8	Saline	Jugular vein	NA	0.3	> 24	NdFeB fixed to the cranium of rats	Effective and tolerable tumor treatment
[51]	10	70–90	Starch-MP GPEI-MP	12	PBS	Tail vein; carotid artery	NA	0.35	0.5	NdFeB (9 mm D) attached to the pole of dipole electromagnet	Targeted vascular drug/gene delivery
[52]	10	70	Starch-MP CMD-MP	12	NA	Tail vein	NA	0.4	0.5	NA	Targeted drug delivery

Table 4 (continued)

Refs.	Nanoparticle administration							Magnetic field			
	Days after induction	Tumor size (mm^3)	Nanoparticle	Dose (mg/kg)	Vehicle	RA	AT (min)	MF (T)	Time of field (h)	Magnet	Application
[53]	10	50–70	Starch-MP	12–25	PBS	Tail vein	NA	0.4	0.5	NA	Applicability of ICP-OES and ESR in MP biodistribution study
[54]	10	NA	Carboxydextran-MP; SPAnH-Epirubicin-MP	NA	NA	Jugular vein	NA	0.2; 0.4; 0.55	3–24	Attached to the animal's scalp, and tightened using a plastic belt	Delivery of nanoparticles to the brain
[55]	10	NA	CMD-MP	10	NA	Jugular vein	NA	0.3	2; 24	Magnet fixed securely to the cranium	Targeted drug delivery
[56]	10	NA	Gum Arabic -MP	12	PBS	Tail vein	NA	NA	0.5	NA	Targeted drug delivery
[57]	10	50–70	Starch-MP	12	PBS	Tail vein	10	0.4	0.5	NA	Targeted drug delivery
[58]	10	50–70	Starch-MP	12	PBS	Tail vein	10	0.4	0.5	NA	Targeted drug delivery
[59]	14–21	NA	Aminodextran-MP; Dextran-MP	4	Tween 80/saline	Carotid artery	2	0.6	0.5	NA	Targeted drug delivery

SPION, superparamagnetic iron oxide nanoparticles; MP, magnetic nanoparticles; AT, administration time; MF, magnetic field; Lf, lactoferrin; Dox, doxorubicin; Cur, curcumin; MDCs, magnetic emulsion nanocapsules; NdFeB, neodymium iron-boron permanent magnet; RA, route administration; S-PEG-β-Glu, starch cross-linked, aminated, PEG modification, conjugation of β-glucosidase; DNPH, aminated, PEGylated, and heparinized D; MT, magnetic targeting; β Glu-S, β-glucosidase to aminated, starch-coated; D, diameter; Dox-SPIO-MBs, doxorubicin-SPIO-circulating microbubbles; BCNU, bischloroethylnitrosourea-loaded nanobubbles; Dx-F-RGD/RGA, Dextrana-Fluorophore-arginine-glycine-aspartate/RGA; SPAnNa, poly[aniline-co-sodium N-(1-one-butyric acid) aniline]; SPAnH, (poly-[aniline-co-N-(1-one-butyric acid) aniline]); PEI, polyethylenimine; PEG, poly(ethylene glycol); Ps 80, Polysorbate 80; GPEI, PEI-modified magnetic nanoparticles coated with gum arabic polysaccharide; CMD, carboxymethyl-dextran; T, Tesla; PBS, phosphate-buffered saline; MRI, magnetic resonance image; ICP-OES, inductively coupled plasma optical emission spectroscopy; ESR, electron spin resonance spectroscopy; NA, not identified; SD-MB, SPIO-doxorubicin-conjugated microbubbles; MFLs, rhodamine-labeled magnetic-fluid-loaded PEG-ylated liposomes.

detection and more targeted treatment [46], more effective and tolerable treatment for cancer [50], applicability of inductively coupled plasma-optical emission spectrometer (ICP-OES) and electron spin resonance (ESR) studies in biodistribution studies of magnetic nanoparticles [53], and effective targeted drug delivery to the brain [54].

Figure 3 shows a schematic of the magnetic targeting process for tumor induction through different routes of SPION administration, the range of the dose used, and its delivery vehicle. In the same figure, the range and time of the external static magnetic field application for further evaluation by different techniques.

3.5 Toxicity

Although physicochemical characterization of SPION was described by studies included in our review of stability of SPION *in vitro*, the viability of the technique to apply SPIONs to tumor was discussed in a few manuscripts as well as the kinetic of biodistribution, elimination of SPION, and *in vivo* toxicity. These constitute the fundamental elements of the magnetic targeting process [47, 51, 53].

External imposition of a static magnetic field for tumor targeting by SPION is better observed in studies on the distribution of SPION in the organism, highlighting the higher concentration of SPION located in the tumor region and its microenvironment. Such fact proved the efficiency of this technique compared with tumor targeting without external magnetic field. Distribution data suggest, indirectly, the viability of the procedure given that the results showed that the physiological route of iron metabolism is maintained, and SPIONs are pushed by the organism, thus, reducing the long-term accumulation of iron in other organs that would turn them toxic [55, 59, 63].

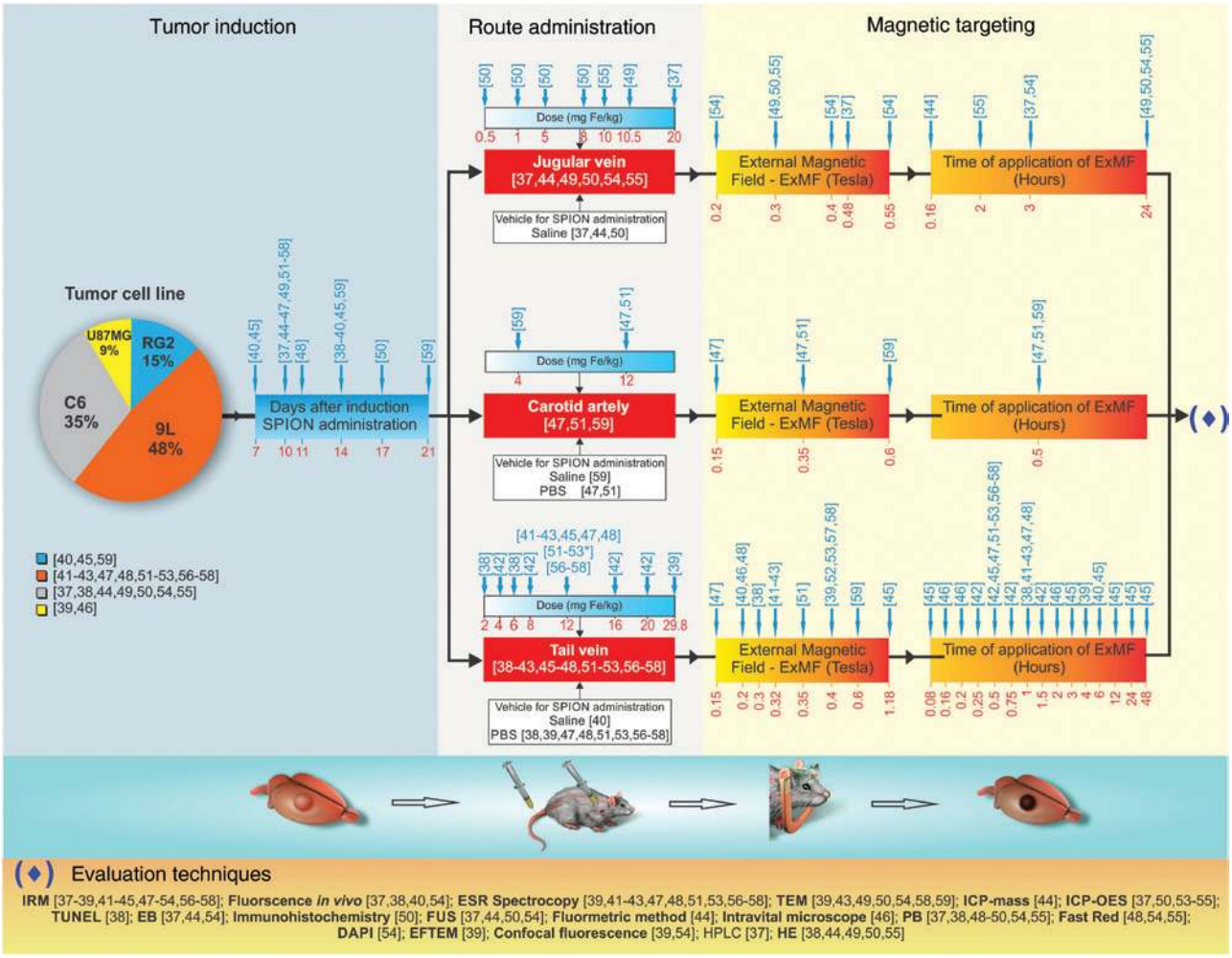

Figure 3: Experimental designs of magnetic targeting process used in the studies selected for the review. *Number of repetitions of ExMF. Studies not mentioned in this figure did not present any of the data items outlined.

Some selected studies, in addition to magnetic targeting technique application, have also applied therapeutic techniques using colorimetric and fluorescent assays and have shown a reduction of *in vivo* or *in vitro* tumor activity. This reduction was observed after tests with different combinations of SPION with different doses of chemotherapy agents and by imposition of external magnetic fields by alternation (generating heat in the tumor area) or not. These studies suggest that specificity of drug delivery to the local of interest using magnetic targeting resource contributes with efficiency to the therapeutic process [40, 43–45, 47, 51].

Despite the clinical and scientific knowledge on the advantages of the low toxicity that therapies with SPIONs present, because of its biocompatibility and possibility of controlling its migration by magnetic resonance imaging, further detailed studies are needed on the biological markers of free radical formation and viability [54]. The imposition of external magnetic field increases the speed and concentration in the migration route of SPION by the bloodstream, and this would cause a toxic effect in the organism. For this reason, detailed analyses are required to guarantee procedure precision to the therapy [54].

In addition, there is also the need to evaluate if imposition of external magnetic field to tumor targeting with SPIONs, even if static, do not cause excessive increase in temperature of acceptable biological heat band, fluctuations of blood pressure, and other secondary effects, therefore, enabling the continuity of homeostasis of the organism.

3.6 Analysis methods

The analysis of the efficiency magnetic targeting in the tumor region can be performed by a set of techniques such as histological assays, immunohistochemical, in *post mortem* tissues, or *ex vivo* and monitoring *in vivo* by MRI. In short, the selected studies address various neuroimaging techniques, illustrated in Table 5, from *in vivo* and *ex vivo* techniques.

Most studies evaluated the magnetic targeting efficiency by MRI technique [37–39, 41–45, 47–54, 56–58]. Of these, 11 studies [39, 41–43, 47, 48, 51, 53, 56–58] also used as an analytical method electron spin resonance (ESR) spectroscopy, transmission electron microscopy (TEM) [39, 43, 49, 50, 54, 58], energy-filtered transmission electron microscopy (EFTEM) [39], focused ultrasound (FUS) [37, 44, 50, 54], fluorometry [44], inductively coupled plasma-mass (ICP-Mass) [44], Evans blue (EB) [37, 44, 54], hematoxylin-eosin (HE) [37, 38, 44, 50], Prussian blue (PB) [37, 38, 49, 50, 54], nuclear fast red (NFR) [48, 54], immunohistochemistry [50], inductively coupled plasma optical emission spectroscopy (ICP-OES) [38, 50, 53, 54], high-performance liquid chromatography (HPLC) [38], confocal/fluorescence microscopy [37–39, 54] or 4′,6-diamidino-2-phenylindole (DAPI) [54], and terminal deoxynucleotidyl transferase dUTP nick-end labeling (TUNEL) [38]. Only four studies did not use MRI with an analytical method [40, 46, 55, 59]. Of these studies, two [40, 46] used fluorescence tomography, and one [55] used intravital microscopy. Huang [55] reported the use of ICP-OES, HE, PB, and NFR, and another study [59] reported the use of MET. Alternative or complementary methods to MRI were mostly performed *ex vivo* [37–44, 47–51, 53–59] using tissue samples for ESR spectroscopy, TEM, fluorometry, ICP-mass, Evans blue, HE, PB, NFR, immunohistochemistry, ICP-OES, and DAPI. Some studies also carried out *in vivo* analyses, such as fluorescence [40], FUS [37, 44, 50, 54], and confocal intravital microscopy [46]/fluorescence microscopy [54].

Among the selected studies, MRI was the main method used for *in vivo* monitoring and targeting by SPION mediated by an external magnetic field to the tumor region. In addition to the accurate images of the different parts of the body, this technique is also advantageous because it is minimally invasive. The intensity range of the MRI equipment used was from 3.0 T [38, 49, 50, 54] to 7.0 T [37, 39, 41–45, 47, 48, 51–53, 56–58]. The most common sequences used were fast-spin-echo (FSE) [41–43, 47, 48, 51–53, 56, 57] and gradient echo (GRE) [39, 41, 43, 44, 47, 48, 50, 51–53, 56–58]. Some studies acquired images only 1 h after magnetic targeting [38, 41–43], while others did temporal measures between 1 and 240 h after targeting [37, 39, 52, 57, 58].

4 Discussion

Brain tumors, especially malignant gliomas, are among the most aggressive human cancers. Despite conventional treatment, which involves surgery, radiation, and chemotherapy, the prognosis is poor, with only 3–5% of patients surviving more than 3 years [64–66]. Furthermore, conventional chemotherapy has several disadvantages, such as low therapeutic efficacy and severe systemic toxicity due to low selectivity for neoplastic cells [67].

To address these drawbacks, drug delivery systems directed to the area of interest have been investigated [68, 69], with particular attention paid to SPIONs [70, 71]. The biocompatible coverage and high magnetic susceptibility of the core make these important compounds candidates

Table 5: Analysis methods.

Refs.	Magnetic resonance imaging						Other methods	
	MF (T)	Sequence	Weighted images: TR(s)/TE (ms)	FOV/MT/ST (mm/–/mm)	Slice separation (mm)	IAT (h)	Technique	Avaliation
[37]	7	NA	T2: 2.54/41	34×40/272×320/0.6	NA	1, 3	FUS	*In vivo*
		Multi-echo	T2: 2/7.1–112	37×60/320×512/0.7	NA	1, 3	HPLC; ICP-OES; EB; HE; PB; fluorescent microscopic imaging	*Ex vivo*
[38]	3	Turbo SE	T2: 2.3/110	56×70/256×256/2.4	2.9	1	Fluorescence; PB; HE; TUNEL	*Ex vivo*
[39]	7	GRE-3D	T2*: 4.095/3.12	150×150×50/192×144×64/NA	NA	4, 8, 24	ESR spectroscopy; confocal fluorescence microscopy; TEM; EFTEM	*Ex vivo*
		RARE	T2: 2.5/33	200×200/128×128/0.8	NA	8, 24		
[40]	NA	NA	NA	NA	NA	NA	Fluorescence	*In vivo*
[41]	7	FSE	T2: 4/60	30×30/128×128/1	2	1	ESR spectroscopy	*Ex vivo*
		GRE	T2: 20×10^{-3}/5					
[42]	7	FSE multi-slice	T2: 4/60	30×30/256×256/1	0	1	ESR spectroscopy	*Ex vivo*
[43]	7	FSE	T2: 4/60	30×30/128×128/1	2	1	ESR spectroscopy, TEM	*Ex vivo*
		GRE	T2: 20×10^{-3}/5					
[44]	7	Echo	T2: 30×10^{-3}/18	34×40/432×512/0.6	NA	0.66, 240	FUS	*In vivo*
		GRE echo-planar	T2*: 1/25	35×35/128×128/0.6			Fluorometric method, ICP-Mass, EB, HE	*EX vivo*
		NA	T2: 2.54/41	34×40/272×320/0.6				
		Multi-echo SE	T2: 2/7.5–120	48×65/320×240/0.7				
[45]	7	Turbo RARE	T2*: 2.5/33	40×40/NA/1	NA	0.5, 3, 6, 12, 24, 48	NA	NA
		Flash	T2: 9.2×10^{-3}/335.1					
[46]	NA	NA	NA	NA	NA	NA	Intravital microscope	*In vivo*
[47]	7	GRE	T2: 20×10^{-3}/5	30×30/12	2	0.5	ESR spectroscopy	*Ex vivo*
		FSE	T2: 4/60	8×128/1				
[48]	7	GRE	T2*: 0.18/5	30×30/128×128/1	0	1, 5, 24	ESR spectroscopy, PB, NFR	*Ex vivo*
		FSE	T2: 4/(30 or 60)	30×30/256×128/1				
[49]	3	NA	T2: 2.51/94	39×60/128×256/NA	NA	0, 168	TEM, PB	*Ex vivo*
[50]	3	Turbo SE	T1: 0.421/11	39×60/128×256/0.7	NA	0, 168	FUS	*In vivo*
		GRE	T2: 2.51/94	39×60/128×256/0.7			TEM, PB, HE, immunohistochemistry, ICP-OES	*Ex vivo*
		GRE	T2*: 28×10^{-3}/20	43×130/128×384/0.7				
[51]	7	FSE	T2: 4×10^{-3}/60	30×30/128×128/1	2	0.5	ESR spectroscopy	*Ex vivo*
		GRE	T2: 20×10^{-3}/5					
[52]	7	FSE	T2: (30 or 60)$\times10^{-3}$/4	30×30/128×128/1	NA	1, 2, 3, 4, 48, 96, 144, 192, 240	NA	NA
		GRE	T2: 20×10^{-3}/5					

Table 5 (continued)

Refs.	Magnetic resonance imaging						Other methods	
	MF (T)	Sequence	Weighted images: TR(s)/TE (ms)	FOV/MT/ST (mm/–/mm)	Slice separation (mm)	IAT (h)	Technique	Avaliation
[53]	7	FSE	T2: 4/60	30×30/128×128/1	2	0.5	ESR spectroscopy, ICP-OES	*Ex vivo*
		GRE	T2: 20×10^{-3}/5					
[54]	3	Turbo SE	T1: 0.78/15	39×60/128×256/1.4	NA	3, 6, 12, 24	FUS, confocal/fluorescence microscopy	*In Vivo*
		Double–TE SE	T2: 3.86/(8/14,28/57,85/228)	38×76/128×256/1.4			TEM, ICP-OES, PB, NFR, DAPI, EB	*Ex vivo*
[55]	NA	NA	NA	NA	NA	NA	ICP-OES, HE, PB, NFR	*Ex vivo*
[56]	7	FSE	T2: 4/60	30×30/128×128/1	1.5	0.5, 240	ESR spectroscopy	*Ex vivo*
		GRE	$T2^*$: 0.275/15					
[57]	7	FSE	T2: (30 or 60)$\times10^{-3}$/4	30×30/128×128/1	NA	1, 2, 3, 4, 48, 96, 144, 192, 240	ESR spectroscopy	*Ex vivo*
		GRE	T2: 20×10^{-3}/5					
[58]	7	GRE	T2: 20×10^{-3}/5	30×30/128×128/1	1.5	1, 2, 3, 4, 48, 96, 144, 192, 240	ESR spectroscopy TEM	*Ex vivo*
		SE	T2: 4/60					
[59]	NA	NA	NA	NA	NA	NA	TEM	*Ex vivo*

MF, magnetic field; TR, repetition time; TE, echo time; T_2, transverse relaxation time; FOV, field-of-view; MT, matrix; ST, Slice thickness; IAT, image acquisition time after magnetofection; FSE, fast-spin-echo; GRE, gradient echo; SE, spin echo; RARE, rapid Imaging with refocused echoes; ESR, electron spin resonance; HPLC, high-performance liquid chromatography; FE-SEM, field emission scanning microscope; TEM, transmission electron microscopy; EFTEM, energy-filtered transmission electron microscopy FUS, focused ultrasound; PB, Prussian blue; NFR, nuclear fast red; HE, hematoxylin-eosin; DAPI, (4′,6-diamidino-2-phenylindole); ICP-Mass, inductively coupled plasma-mass; ICP-OES, inductively coupled plasma optical emission spectroscopy; TUNEL, terminal deoxynucleotidyl transferase dUTP nick-end labeling; NA, not identified.

for drug delivery or drug target vehicles. Furthermore, the polymer coating provides the possibility for conjugation of additional functional groups, as well as allows, at the same time, magnetic targeting to tumor and monitoring by MRI [56, 57, 70–72].

The use of an external magnetic field for targeting compounds to specific sites has been reported for decades; it was initially done with microspheres [73–75]. The attraction by an external magnetic field allows active targeting into tumor. This is a particularly attractive technique for gliomas because of the difficult location of these tumors. Despite the enhanced permeability and retention effect (EPR) reported in solid tumors, allowing the nanoparticles to accumulate passively in tumor interstice [63, 76–78], the active targeting significantly increases exposure to the tumor [57].

SPION coating with biomaterials evidence the potential toxicity effects regarding shape, size, and surface characteristics of nanoparticles; however, because of divergence and speculation regarding the analysis of these characteristics, it is very difficult to establish the toxic effects related to these SPION properties [79]. Despite the lack of evidence in toxicity of SPIONs, information regarding the possible risk of SPION exposure to humans is still very limited and conflicting. The potential toxic effects of SPION is mainly focused on evaluating cytotoxic effects, especially changes in viability, cytoskeleton disruptions, ROS production, and *in vitro* cell cultures [80]. Little is known about the iron toxicity to genetic material, the nervous system, embryonic development, and other endpoints [81]. A review using SPION-labeled cells in regenerative therapies did not report cytotoxic effects for these nanoparticles [82]. In addition, no significant toxicity and successful chondrogenesis occurred in human mesenchymal stem cells incubated for 24 or 72 h with ferucarbotran (a clinically approved and commercially available carboxydextran-coated SPION that is used as a negative MRI contrast agent for hepatic imaging) [83]. These reviews and other studies show lack of evidence to low toxicity of SPIONs *in vitro* biological assay and *in vivo*, or in preclinical studies.

In addition, there is scientific and clinical evidence that SPION therapies have advantages such as low toxicity and also present biocompatibility and the possibility of control migration by the MRI [78, 84]. In this context, a search was made for studies that used optimization strategies for the delivery of iron oxide nanoparticles magnetically targeted for tumor lesions using experimental glioma models. Although 23 studies were found within the established prerequisites, they belong to a total of nine research groups. Most publications belong to the group coordinated by Victor Yang (10 out of 23, 46%), followed by Kuo-Wei Chen (4 out of 23, 17%).

Analysis of the accuracy of magnetic targeting process begins with tumor induction in different locations by different cell lines and cell concentrations in selected studies. Afterward, the nanoparticle administration is made by different routes, in different concentrations on different days standardized in each study, for later application of an external magnetic field with different strengths, times, and adjustments, aiming these nanoparticles for targeting to the tumor lesion. Subsequently, it was also compared to the different analysis methods of the targeting efficiency, as is shown in Figure 3.

In this context, and compared with a recent review [62], our review about rat brain tumor models in experimental neuro-oncology, which describes the differences in eight brain tumor lineages in rodent model (C6, 9L, T9, RG2, F98, BT4C, RT-2, CNS-1), allowed to show the difference in route of administration, highlighting that caudal is the most common local used for C6, 9L, BT4C, and RT-2, but intracerebral was the most common for F98 and CNS-1, a result that corroborates with selected studies shown in Figure 3. There are studies with subdermal implantation or animal flank for optimization of SPION magneto driving and tumor growth in other cancer models. However, the blood-brain barrier constitutes a limit for a number of therapeutic drugs and methods because it does not allow infiltration of anything, including drugs. The stereotactic or flank implantation keeps the general principles of tumor cell implantation, but it turns the accuracy of therapeutic outcomes easier or fake in some cancer models. The C6, 9L, and RT-2 are solid and circumscribed tumors. The other tumors are not circumscribed, and they present several degrees of infiltrating capacity of contiguous normal brain with or without islands of tumor cells with distance varying from the core tumor mass. These cancer models pose more difficulty in measuring the accuracy of therapies, including the nanoparticle therapy [62].

The magnetic targeting technique is not new, as the first identified publication was in 1999 [59]. In the selected publications, the use of commercial compounds was equilibrated with the use of the synthesized compounds in the laboratory. Among the studies that used commercial compounds, the majority used FluidMAG-D, coated with starch (15 out of 23, 67%). Another interesting fact is that almost half of the studies used more than one type of nanoparticle to compare the targeting efficiency (9 out of 23, 75%). Of these, about half (4 out of 9, 45%) compared the efficiency of commercial compounds with nanoparticles synthesized by the group, 45% (4 out of 9) compared different synthesized compounds, and only one study

compared the efficiency of only commercial compounds. All used nanoparticles had magnetite core and generally had small hydrodynamic size (most with 100–110 nm; 14 out of 23, 64%).

The main cell line used for tumor induction was 9L cells, described in all Yang's studies (11 out of 23, 45%). These cells are able to generate a gliosarcoma tumor in rats, mimicking important human tumor characteristics, such as the pattern of tumor growth and metastasis. The second most used was the C6 cell line, a model widely used for a variety of studies on tumor growth, invasion, migration, neovascularization, growth factor regulation, and biochemical studies, being morphologically similar to glioblastoma multiforme [61, 62]. DMEM was the main culture medium used for cell proliferation for tumor induction (13 out of 23, 55%).

Most studies used rats as an animal model for tumor induction (15 out of 23, 75%); the most commonly used species was the Fisher 344 rat (9 of 23, 45%). The number of cells also varied, with the most-used concentration 10^6 cells inoculated directly into the right hemisphere of the brain (7 out of 23, 35%). The main vehicle suspension used for tumor cells was DMEM without serum (11 of 23, 55%).

All studies included in our review showed that application of a static external magnetic field at some level of intensity (0.2–1.18 T) and at some period (0.25–24 h) was enough to increase the nanoparticle concentration in the tumor region compared with non-targeted animals.

For Zhou [41], the conjugation with PEG to increase the stability of the nanoparticles and β-glucosidase enzyme with great effect in killing tumor cells led to a 3.6-fold greater accumulation into the tumor region when applying a magnetic field compared with other groups without targeting. These results corroborate with the previous study [43] in which evidence that the nanoparticle accumulation 60 min after administration was selective for tumor site and increased 3.84-fold nanoparticle concentration in targeted groups that compared with animals without magnetic targeting. Cole [48] also showed an increase of 189- to 229-fold more nanoparticles conjugated with PEG by an external magnetic field in comparison to commercial nanoparticles distributed passively to the tumor.

The success of the magnetic targeting is determined by three factors: intensity of the applied magnetic field, physicochemical properties of the nanoparticles, and stability of these compounds in the bloodstream. Based on this, Zhang's study [42] examined the influence of the administration route on optimizing the magnetic targeting process; they showed greater therapeutic effectiveness when SPIONs are administered by carotid artery. At a dose of 12 mg Fe/ml and after applying a magnetic field for 45 min, a 200-fold greater accumulation in the tumor region was reported compared with the group using a commercial nanoparticle and non-targeted. Chertok [47] also demonstrated the importance of the administration route, reporting greater nanoparticle exposure in tumor vasculature when administered by carotid. In his study, the nanoparticle aggregation in tumor was 1.8-fold higher when these were administered by intra-arterial route compared to intravenous administration, both with magnetic targeting.

Chertok [51] also tested the applicability of nanoparticles conjugated with PEI to increase retention and vascular drug carriers, using carotid artery for administration in order to decrease the loss of the drug. The influence of the administration route was also studied demonstrating an advantage of 30-fold more nanoparticle aggregation in the tumor comparing carotid to intravenous administration, both subjected to magnetic targeting process. The nanoparticles conjugated with PEI also showed advantages compared to the commercial compound, adding a 5.2-fold higher accumulation in the tumor as magnetically targeted.

The study by Fan [44] used a combination of ultrasound technique with the application of a magnetic field and showed a synergistic effect in nanoparticle accumulation (22.4%) compared with the group without a magnetic field (12%). The same was shown by Chen [50]. In his study, when the magnetic field or ultrasound was applied alone, twofold more SPION accumulation occurred in the tumor region. Therefore, the combination of techniques increases aggregation in tumor 26 times. Also in Liu's study [54], the combination of these techniques showed an increase in nanoparticle concentration of 244.6% into the tumor area rather than into the adjacent brain tissue. Huan's study [55] showed that as a consequence of magnetic targeting, nanoparticles were more directed to the brain, reducing the dispersion in other organs as the lungs, liver, kidneys, and spleen. Therefore, the use of 0.5 T of magnetic field for 30 min and single ultrasound of 500 KHz were more effective drug or magneto carrier in the selected studies.

Huang's study [45] evidenced significant tumor reduction associated with the nanoparticle administration with BCNU and together with an external field, showing that the magnetic targeting increases the tumor exposure and decreases its concentration in the bloodstream, also reducing the toxic effects. In addition, there were more nanoparticle retention and internalization in the tumor by applying the magnetic field (two fold more signal strength after 30 s). Fu [46] in his study also showed the effect of

magnetic targeting process in tumor regression, which occurred faster with the use of magnetic targeting due to the higher concentration of nanoparticles conjugated with RDG (antitumor agent) into the tumor locus. Hua [49] also observed a tumor inhibition growth when SPION conjugated with BCNU were magnetically targeted to the tumor region. The Increase in the SPION concentration into the tumor locus using an external magnetic field makes it possible to use a lower dose of drug to promote tumor suppression and reducing systemic adverse effects.

Yu [52] also compared the efficiency of magnetic targeting using commercial nanoparticles and synthesized nanoparticles. It presented advantages over commercial compounds due to more mobility with a magnetic field and effective accumulation in the tumor region. Zhang [56] also compared both commercial and synthesized nanoparticles, conjugating gum arabic to stabilize the nanoparticles, and adding the fluorophore rhodamine B. As a result of magnetic targeting, there was eightfold more nanoparticle aggregation in the tumor when compared to the group without magnetic targeting. The oldest selected study also compared different compounds. Contrary to what occurs in the 1000- to 2000-nm microspheres, there was better magnetic targeting in approximately 10–20 nm nanoparticles. In addition, the imposition of an external magnetic field permitted the accumulation of 41–48% of the all iron dose into tissue between 30 min to 6 h of targeting. Without magnetic targeting, only 31–32% of the dose was accumulated in the tumor locus.

In another, the study by Chertok [57] showed that the imposition of a magnetic field allowed an increase of five times the drug concentration into the tumor area compared to non-targeted animals. Furthermore, the targeting of nanoparticles in the tumor locus persisted for approximately 100 min after the magnet removal. The selectivity retention of the glioma locus relative to the contralateral brain region was also analyzed by Chertok [58]. This study found a 9.6-fold higher retention into the glioma site. In another study by Chertok [53], he only tested the ESR and ICP-OES efficiency quantification of nanoparticles into the tumor region after application of an external magnetic field.

The most common analysis method to check the efficiency of magnetic targeting was the MRI technique identified in 16 studies (80%). Among the various forms of *in vivo* targeting, MRI is considered an important tool that is non-invasive, with high spatial resolution, without exposure to ionizing radiation, and allows information about the nanoparticle accumulation in the tumor region, from T2-weighted. It allows obtaining real-time images with morphological and functional information at the cellular and molecular level, helping in understanding the migration of nanoparticles guided by an external magnetic field. Other methods that have been widely used are ESR spectroscopy (10 out of 23, 48%), MET (6 out of 23, 30%), and ICP-OES (4 out of 23, 20%), important for nanoparticle quantification and visualization. Less than half of the studies used histological methods to verify the magnetic targeting (6 out of 23, 27%).

In clinical trials about magnetic targeting using SPIONs and other magneto nanoparticles for driving or carrier drugs, therapeutic pitfalls or collateral effects were reported lower, and the toxicity was also low [33, 34, 85]. The clinical trial that used SPION in cancer [33] included seven metastatic breast cancer patients who underwent magnetic field (0.4 T) application near the tumor area twice a day, 3 days per week for 6 weeks, presented SPIONs increased in three fields into the tumor. The comparison done without magneto application showed no hematological effects and toxicity. Other studies produced the same results of the first clinical trial, but an increase in concentration into the tumor area and lower SPION concentration were seen using intravenous administration in the area near the tumor.

According to the data presented here, nanobiotechnology is presented as a powerful tool for the development of magnetically guided nanoplatforms, which ensures a more effective treatment that can be directed to high-grade gliomas and together with MRI allows *in vivo* tracking. However, because of the complexity of the central nervous system, the magnetic targeting process is still a challenge, and tools in the field of nanomedicine to survey and guide these studies are highly desirable.

Acknowledgments: This study was supported by the Albert Einstein Jewish Institute for Education and Research (Instituto Israelita de Ensino e Pesquisa Albert Einstein – IIEPAE), the National Council for Scientific and Technological Development (Conselho Nacional de Desenvolvimento Científico e Tecnológico – CNPq), the Studies and Projects Financing Agency (Financiadora de Estudos e Projetos – FINEP), the Brazilian Federal Agency for the Support and Evaluation of Graduate Education (Coordenação de Aperfeiçoamento de Pessoal de Nível Superior – CAPES), and the São Paulo State Research Support Foundation (Fundação de Amparo à Pesquisa do Estado de São Paulo – FAPESP).

Competing interest of statement: The authors declare no competing interests. All authors read and approved the final manuscript.

References

[1] Stylli SS, Luwor RB, Ware TM, Tan F, Kaye AH. Mouse models of glioma. *J. Clin. Neurosci.* 2015, 22, 619–626.

[2] Lim SK, Llaguno SR, McKay RM, Parada LF. Glioblastoma multiforme: a perspective on recent findings in human cancer and mouse models. *BMB Rep.* 2011, 44, 158–164.

[3] de Vries NA, Beijnen JH, van Tellingen O. High-grade glioma mouse models and their applicability for preclinical testing. *Cancer Treat. Rev.* 2009, 35, 714–723.

[4] Hu X, Holland EC. Applications of mouse glioma models in preclinical trials. *Mutat. Res.* 2005, 576, 54–65.

[5] Burton EC, Prados MD. Malignant gliomas. *Curr. Treat. Options Oncol.* 2000, 1, 459–468.

[6] Adamson DC, Rasheed BA, McLendon RE, Bigner DD. Central nervous system. *Cancer Biomark.* 2010, 9, 193–210.

[7] CBTRUS statistical report: primary brain and central nervous system tumors diagnosed in the United States in 2007–2011. 2014, 16.

[8] Louis DN, Ohgaki H, Wiestler OD, Cavenee WK, Burger PC, Jouvet A, Scheithauer BW, Kleihues P. The 2007 WHO classification of tumours of the central nervous system. *Acta Neuropathol*. 2007, 114, 97–109.

[9] Castro MG, Cowen R, Williamson IK, David A, Jimenez-Dalmaroni MJ, Yuan X, Bigliari A, Williams JC, Hu J, Lowenstein PR. Current and future strategies for the treatment of malignant brain tumors. *Pharmacol. Ther.* 2003, 98, 71–108.

[10] Chiocca EA. Oncolytic viruses. *Nat. Rev. Cancer* 2002, 2, 938–950.

[11] Curtin JF, King GD, Candolfi M, Greeno RB, Kroeger KM, Lowenstein PR, Castro MG. Combining cytotoxic and immune-mediated gene therapy to treat brain tumors. *Curr. Top. Med. Chem.* 2005, 5, 1151–1170.

[12] Gomez-Manzano C, Yung WK, Alemany R, Fueyo J. Genetically modified adenoviruses against gliomas: from bench to bedside. *Neurology* 2004, 63, 418–426.

[13] Castro MG, Candolfi M, Kroeger K, King GD, Curtin JF, Yagiz K, Mineharu Y, Assi H, Wibowo M, Ghulam Muhammad AK, Foulad D, Puntel M, Lowenstein PR. Gene therapy and targeted toxins for glioma. *Curr Gene Ther.* 2005, 5, 535–557.

[14] Prados MD, Levin V. Biology and treatment of malignant glioma. *Semin. Oncol.* 2000, 27, 1–10.

[15] Muldoon LL, Soussain C, Jahnke K, Johanson C, Siegal T, Smith QR, Hall WA, Hynynen K, Senter PD, Peereboom DM, Neuwelt EA. Chemotherapy delivery issues in central nervous system malignancy: a reality check. *J. Clin. Oncol.* 2007, 25, 2295–2305.

[16] Juillerat-Jeanneret L. The targeted delivery of cancer drugs across the blood-brain barrier: chemical modifications of drugs or drug-nanoparticles? *Drug Discov. Today* 2008, 13, 1099–1106.

[17] Sheikov N, McDannold N, Sharma S, Hynynen K. Effect of focused ultrasound applied with an ultrasound contrast agent on the tight junctional integrity of the brain microvascular endothelium. *Ultrasound Med. Biol.* 2008, 34, 1093–1104.

[18] Motl S, Zhuang Y, Waters CM, Stewart CF. Pharmacokinetic considerations in the treatment of CNS tumours. *Clin. Pharmacokinet.* 2006, 45, 871–903.

[19] Heimberger AB, Archer GE, McLendon RE, Hulette C, Friedman AH, Friedman HS, Bigner DD, Sampson JH. Temozolomide delivered by intracerebral microinfusion is safe and efficacious against malignant gliomas in rats. *Clin. Cancer Res.* 2000, 6, 4148–4153.

[20] Gutman RL, Peacock G, Lu DR. Targeted drug delivery for brain cancer treatment. *J. Control. Release* 2000, 65, 31–41.

[21] Louis DN, Pomeroy SL, Cairncross JG. Focus on central nervous system neoplasia. *Cancer Cell* 2002, 1, 125–128.

[22] Ohgaki H, Kleihues P. Population-based studies on incidence, survival rates, and genetic alterations in astrocytic and oligodendroglial gliomas. *J. Neuropathol. Exp. Neurol.* 2005, 64, 479–489.

[23] Riemenschneider MJ, Jeuken JW, Wesseling P, Reifenberger G. Molecular diagnostics of gliomas: state of the art. *Acta Neuropathol.* 2010, 120, 567–584.

[24] Meng XX, Wan JQ, Jing M, Zhao SG, Cai W, Liu EZ. Specific targeting of gliomas with multifunctional superparamagnetic iron oxide nanoparticle optical and magnetic resonance imaging contrast agents. *Acta Pharmacologica* 2007, 28, 2019–2007.

[25] Bakhtiary Z, Saei AA, Hajipour MJ, Raoufi M, Vermesh O, Mahmoudi M. Targeted superparamagnetic iron oxide nanoparticles for early detection of cancer: possibilities and challenges. *Nanomed.: Nanotechnol. Biol. Med*. 2016, 12, 287–307.

[26] Gobbo OL, Sjaastad K, Radomski MW, Volkov Y, Prina-Mello A. Magnetic nanoparticles in cancer theranostics. *Theranostics* 2015, 5, 1249.

[27] Bull E, Madani SY, Sheth R, Seifalian A, Green M, Seifalian AM. Stem cell tracking using iron oxide nanoparticles. *Int. J. Nanomedicine* 2014, 9, 1641–1653.

[28] Wegscheid ML, Morshed RA, Cheng Y, Lesniak MS. The art of attraction: applications of multifunctional magnetic nanomaterials for malignant glioma. *Exp. Opin. Drug Deliv.* 2014, 11, 957–975.

[29] Wanga M, Thanoua M. Targeting nanoparticles to cancer. *Pharmacol. Res*. 2010, 62, 90–99.

[30] Bazak R, Houri M, El Achy S, Kamel S, Refaat T. Cancer active targeting by nanoparticles: a comprehensive review of literature. *J. Cancer Res. Clin. Oncol*. 2015, 141, 769–784.

[31] Yeh JS, Sennoga CA, McConnell E, Eckersley R, Tang MX, Nourshargh S, Seddon JM, Haskard DO, Nihoyannopoulos P. A targeting microbubble for ultrasound molecular imaging. *PLoS One* 2015, 10, e0129681.

[32] Sensenig R, Sapir Y, MacDonald C, Cohen S, Polyak B. Magnetic nanoparticle-based approaches to locally target therapy and enhance tissue regeneration in vivo. *Nanomedicine (Lond)* 2012, 7, 1425–1442.

[33] Lübbe AS, Bergemann C, Riess H, Schriever F, Reichardt P, Possinger K, Matthias M, Dörken B, Herrmann F, Gürtler R, Hohenberger P, Haas N, Sohr R, Sander B, Lemke AJ, Ohlendorf D, Huhnt W, Huhn D. Clinical experiences with magnetic drug targeting: a phase I study with 4′-epidoxorubicin in 14 patients with advanced solid tumors. *Cancer Res.* 1996, 56, 4686–4693.

[34] Lübbe AS, Alexiou C, Bergemann C. Clinical applications of magnetic drug targeting. *J. Surg. Res.* 2001, 95, 200–206.

[35] Maher EA, Furnari FB, Bachoo RM, Rowitch DH, Louis DN, Cavenee WK, DePinho RA. Malignant glioma: genetics and biology of a grave matter. *Genes Dev.* 2001, 15, 1311–1333.

[36] Kleihues P, Zülch KJ, Matsumoto S, Radke U. Morphology of malignant gliomas induced in rabbits by systemic application of N-methyl-N-nitrosourea. *Z. Neurol.* 1970, 198, 65–78.
[37] Fan C, Cheng Y, Ting C, Ho Y, Hsu P, Liu H. Ultrasound/magnetic targeting with SPIO-DOX-microbubble complex for image-guided drug delivery in brain tumors. *Theranostics* 2016, 6, 1542–1556.
[38] Xu H, Mao K, Huang Y, Yang J, Xu J, Chen P, Fan ZL, Zou S, Gao ZZ, Yin JY, Xiao J, Lu CT, Zhang BL, Zhao YZ. Glioma-targeted superparamagnetic iron oxide nanoparticles as drug-carrying vehicles for theranostic effects. *Nanoscale* 2016, 8, 14222–14236.
[39] Marie H, Lemaire L, Franconi F, Lajnef S, Frapart Y, Nicolas V, Frébourg G, Trichet M, Ménager C, Lesieur S. Superparamagnetic liposomes for MRI monitoring and external magnetic field-induced selective targeting of malignant brain tumors. *Adv. Funct. Mater*. 2015, 25, 1258–1269.
[40] Fang JH, Lai YH, Chiu TL, Chen YY, Hu SH, Chen SY. Magnetic core-shell nanocapsules with dual targeting capabilities and co delivery of multiple drugs to treat brain gliomas. *Adv. Healthc. Mater.* 2014, 3, 1250–1260.
[41] Zhou J, Zhang J, Gao W. Enhanced and selective delivery of enzyme therapy to 9L-glioma tumor via magnetic targeting of PEG-modified, β-glucosidase-conjugated iron oxide nanoparticles. *Int. J. Nanomedicine* 2014, 9, 2905–2917.
[42] Zhang J, Shin MC, Yang VC. Magnetic targeting of novel heparinized iron oxide nanoparticles evaluated in a 9L-glioma mouse model. *Pharm, Res.* 2014, 31, 579–592.
[43] Zhou J, Zhang J, David AE, Yang VC. Magnetic tumor targeting of β-glucosidase immobilized iron oxide nanoparticles. *Nanotechnology* 2013, 24, 375102.
[44] Fan CH, Ting CY, Lin HJ, Wang CH, Liu HL, Yen TC, Yeh CK. SPIO-conjugated, doxorubicin-loaded microbubbles for concurrent MRI and focused-ultrasound enhanced brain-tumor drug delivery. *Biomaterials* 2013, 34, 3706–3715.
[45] Huang HY, Hu SH, Hung SY, Chiang CS, Liu HL, Chiu TL, Lai HY, Chen YY, Chen SY. SPIO nanoparticle-stabilized PAA-F127 thermosensitive nanobubbles with MR/US dual-modality imaging and HIFU-triggered drug release for magnetically guided in vivo tumor therapy. *J. Control. Release* 2013, 172, 118–127.
[46] Fu A, Wilson RJ, Smith BR, Mullenix J, Earhart C, Akin D, Guccione S, Wang SX, Gambhir SS. Fluorescent magnetic nanoparticles for magnetically enhanced cancer imaging and targeting in living subjects. *ACS Nano* 2012 Aug 28, 6, 6862–6869.
[47] Chertok B, David AE, Yang VC. Brain tumor targeting of magnetic nanoparticles for potential drug delivery: effect of administration route and magnetic field topography. *J. Control. Release.* 2011, 155, 393–399.
[48] Cole AJ, David AE, Wang J, Galbán CJ, Yang VC. Magnetic brain tumor targeting and biodistribution of long-circulating PEG-modified, cross-linked starch-coated iron oxide nanoparticles. *Biomaterials* 2011, 32, 6291–6301.
[49] Hua MY, Liu HL, Yang HW, Chen PY, Tsai RY, Huang CY, Tseng IC, Lyu LA, Ma CC, Tang HJ, Yen TC, Wei KC. The effectiveness of a magnetic nanoparticle-based delivery system for BCNU in the treatment of gliomas. *Biomaterials* 2011, 32, 516–527.
[50] Chen PY, Liu HL, Hua MY, Yang HW, Huang CY, Chu PC, Lyu LA, Tseng IC, Feng LY, Tsai HC, Chen SM, Lu YJ, Wang JJ, Yen TC, Ma YH, Wu T, Chen JP, Chuang JI, Shin JW, Hsueh C, Wei KC. Novel magnetic/ultrasound focusing system enhances nanoparticle drug delivery for glioma treatment. *Neuro Oncol.* 2010, 12, 1050–1060.
[51] Chertok B, David AE, Yang VC. Polyethyleneimine-modified iron oxide nanoparticles for brain tumor drug delivery using magnetic targeting and intra-carotid administration. *Biomaterials* 2010, 31, 6317–6324.
[52] Yu F, Zhang L, Huang Y, Sun K, David AE, Yang VC. The magnetophoretic mobility and superparamagnetism of core-shell iron oxide nanoparticles with dual targeting and imaging functionality. *Biomaterials* 2010, 31, 5842–5848.
[53] Chertok B, Cole AJ, David AE, Yang VC. Comparison of electron spin resonance spectroscopy and inductively-coupled plasma optical emission spectroscopy for biodistribution analysis of iron-oxide nanoparticles. *Mol. Pharm.* 2010, 7, 375–385.
[54] Liu HL, Hua MY, Yang HW, Huang CY, Chu PC, Wu JS, Tseng IC, Wang JJ, Yen TC, Chen PY, Wei KC. Magnetic resonance monitoring of focused ultrasound/magnetic nanoparticle targeting delivery of therapeutic agents to the brain. *Proc. Natl. Acad. Sci. USA* 2010, 107, 15205–15210.
[55] Huang BR, Chen PY, Huang CY, Jung SM, Ma YH, Wu T, Chen JP, Wei KC. Bioavailability of magnetic nanoparticles to the brain. *J. Magn. Magn. Mater.* 2009, 312, 1604–1609.
[56] Zhang L, Yu F, Cole AJ, Chertok B, David AE, Wang J, Yang VC. Gum arabic-coated magnetic nanoparticles for potential application in simultaneous magnetic targeting and tumor imaging. *AAPS J.* 2009, 11, 693–699.
[57] Chertok B, Moffat BA, David AE, Yu F, Bergemann C, Ross BD, Yang VC. Iron oxide nanoparticles as a drug delivery vehicle for MRI monitored magnetic targeting of brain tumors. *Biomaterials* 2008, 29, 487–496.
[58] Chertok B, David AE, Huang Y, Yang VC. Glioma selectivity of magnetically targeted nanoparticles: a role of abnormal tumor hydrodynamics. *J. Control. Release* 2007, 122, 315–323.
[59] Pulfer SK, Ciccotto SL, Gallo JM. Distribution of small magnetic particles in brain tumor-bearing rats. *J. Neurooncol.* 1999, 41, 99–105.
[60] Benda P, Lightbody J, Sato G, Levine L, Sweet W. Differentiated rat glial cell strain in tissue culture. *Science* 1968, 161, 370–371.
[61] Grobben B, De Deyn PP, Slegers H. Rat C6 glioma as experimental model system for the study of glioblastoma growth and invasion. *Cell Tissue Res.* 2002, 310, 257–270.
[62] Barth RF, Kaur B. Rat brain tumor models in experimental neuro-oncology: the C6, 9L, T9, RG2, F98, BT4C, RT-2 and CNS-1 gliomas. *J. Neurooncol.* 2009, 94, 299–312.
[63] Maeda H, Bharate GY, Daruwalla J. Polymeric drugs for efficient tumor-targeted drug delivery based on EPR-effect. *Eur. J. Pharm. Biopharm.* 2009, 71, 409–419.
[64] Aoki T, Hashimoto N, Matsutani M. Management of glioblastoma. *Exp. Opin. Pharmacother.* 2007, 8, 3133–3146.
[65] Maher EA, Mietz J, Arteaga CL, DePinho RA, Mohla S. Brain metastasis: opportunities in basic and translational research. *Cancer Res.* 2009, 69, 6015–6020.
[66] Krex D, Klink B, Hartmann C, von Deimling A, Pietsch T, Simon M, Sabel M, Steinbach JP, Heiese O, Reifenberger G, Weller M, Schackert G. German GliomaNetwork. Long-term survival with glioblastoma multiforme. *Brain* 2007, 130, 2596–2606.
[67] Lindley C, McCune JS, Thomason TE, Lauder D, Sauls A, Adkins S, Sawyer WT. Perception of chemotherapy side effects cancer versus noncancer patients. *Cancer Pract.* 1999, 7, 59–65.

[68] Sawant RM, Hurley JP, Salmaso S, Kale A, Tolcheva E, Levchenko TS, Torchilin VP. "SMART" drug delivery systems: double-targeted pH-responsive pharmaceutical nanocarriers. *Bioconjug. Chem.* 2006, 17, 943–949.
[69] Winer I, Wang S, Lee YE, Fan W, Gong Y, Burgos-Ojeda D, Spahlinger G, Kopelman R, Buckanovich RJ. F3-targeted cisplatin-hydrogel nanoparticles as an effective therapeutic that targets both murine and human ovarian tumor endothelial cells in vivo. *Cancer Res.* 2010, 70, 8674–8683.
[70] Xie J, Liu G, Eden HS, Ai H, Chen X. Surface-engineered magnetic nanoparticle platforms for cancer imaging and therapy. *Acc. Chem. Res.* 2011, 44, 883–892.
[71] Reddy LH, Arias JL, Nicolas J, Couvreur P. Magnetic nanoparticles: design and characterization, toxicity and biocompatibility, pharmaceutical and biomedical applications. *Chem. Rev.* 2012, 112, 5818–5878.
[72] Yoo D, Lee JH, Shin TH, Cheon J. Theranostic magnetic nanoparticles. *Acc. Chem. Res.* 2011, 44, 863–874. Erratum in: *Acc Chem Res.* 2012, 45, 1622.
[73] Widder KJ, Senyel AE, Scarpelli GD. Magnetic microspheres: a model system of site specific drug delivery in vivo. *Proc. Soc. Exp. Biol. Med.* 1978, 158, 141–146.
[74] Widder KJ, Senyei AE. Magnetic microspheres: a vehicle for selective targeting of drugs. *Pharmacol. Ther.* 1983, 20, 377–395.
[75] Gupta PK, Hung CT. Magnetically controlled targeted microcarrier systems. *Life Sci.* 1989, 44, 175–186.
[76] Chandran SS, Banerjee SR, Mease RC, Pomper MG, Denmeade SR. Characterization of a targeted nanoparticle functionalized with a urea-based inhibitor of prostate-specific membrane antigen (PSMA). *Cancer Biol. Ther.* 2008, 7, 974–982.
[77] Maeda H, Wu J, Sawa T, Matsumura Y, Hori K. Tumor vascular permeability and the EPR effect in macromolecular therapeutics: a review. *J. Control. Release* 2000, 65, 271–284.
[78] Maier-Hauff K, Ulrich F, Nestler D, Niehoff H, Wust P, Thiesen B, Orawa H, Budach V, Jordan A. Efficacy and safety of intratumoral thermotherapy using magnetic iron-oxide nanoparticles combined with external beam radiotherapy on patients with recurrent glioblastoma multiforme. *J. Neurooncol.* 2011, 103, 317–324.
[79] Patil US, Adireddy S, Jaiswal A, Mandava S, Lee BR, Chrisey DB. In vitro/in vivo toxicity evaluation and quantification of iron oxide nanoparticles. *Int. J. Mol. Sci.* 2015, 16, 24417–24450.
[80] Valdiglesias V, Kiliç G, Costa C, Fernández-Bertólez N, Pásaro E, Teixeira JP, Laffon B. Effects of iron oxide nanoparticles: cytotoxicity, genotoxicity, developmental toxicity, and neurotoxicity. *Environ. Mol. Mutagen*. 2015, 56, 125–148.
[81] Au KW, Liao SY, Lee YK, Lai WH, Ng KM, Chan YC, Yip MC, Ho CY, Wu EX, Li RA, Siu CW, Tse HF. Effects of iron oxide nanoparticles on cardiac differentiation of embryonic stem cells. *Biochem. Biophys. Res. Commun*. 2009, 379, 898–903.
[82] Alvarim LT, Nucci LP, Mamani JB, Marti LC, Aguiar MF, Silva HR, Silva GS, Nucci-da-Silva MP, DelBel EA, Gamarra LF. Therapeutics with SPION-labeled stem cells for the main diseases related to brain aging: a systematic review. *Int. J. Nanomedicine* 2014, 9, 3749–3770.
[83] Yang CY, Hsiao JK, Tai MF, Chen ST, Cheng HY, Wang JL, Liu HM. Direct labeling of hMSC with SPIO: the long-term influence on toxicity, chondrogenic differentiation capacity, and intracellular distribution. *Mol. Imaging Biol*. 2011, 13, 443–451.
[84] Kim BYS, Rutka JT, Chan WCW. Nanomedicine. Review Article. *N. Engl. J. Med.* 2010, 363, 2434–2443.
[85] Johnson J, Kent T, Koda J, Peterson C, Rudge S, Tapolsky G. The MTC technology: a platform technology for the site-specific delivery of pharmaceutical agents. *Eur. Cells Mater*. 2002, 3, 12–15.

Bionotes

Marina Fontes de Paula Aguiar
Hospital Israelita Albert Einstein, São Paulo, Brazil; and Universidade Federal de São Paulo, Unifesp, São Paulo, Brazil

Marina Fontes de Paula Aguiar received her bachelor degree in Biology from UNESP, Brazil, in 2011 and her Master Degree in Neuroscience from UNIFESP, Brazil, in 2015 that resulted in a national patent. She has experience in Nanotechnology and Cellular and Molecular biology with emphasis in therapeutic strategies for glioblastoma brain tumor using nanobiotechnological tools. Her researches included the use of glioma animal models to develop strategies for treatment of brain tumors using iron oxide nanoparticles and magnetic targeting.

Javier Bustamante Mamani
Hospital Israelita Albert Einstein, São Paulo, Brazil

Javier Bustamante Mamani obtained his PhD from the University of São Paulo in Brazil in 2009. He is currently doing a postdoctoral study on nanobiotechnology at the Israelite Albert Einstein Hospital. His research interests include the elaboration, the physicochemical and biological studies, and the *in vivo* application of iron oxide nanoparticles for magnetic hyperthermia.

Taylla Klei Felix
Hospital Israelita Albert Einstein, São Paulo, Brazil

Taylla Klei Felix received his Technologist in Radiology degree from the Ipiranga Integrated Colleges in 2012. Nowadays, he conducts research at the Hospital Israelita Albert Einstein in the Brain Institute, developing research in animal models using iron oxide nanoparticles to application in glioblastomas with magnetic hyperthermia therapy, analyzing the efficiency by bioluminescence techniques, MRI, and histology.

Rafael Ferreira dos Reis
Hospital Israelita Albert Einstein, São Paulo, Brazil; and Universidade Federal de São Paulo, Unifesp, São Paulo, Brazil

Rafael Ferreira dos Reis has a Biomedical degree from the Mogi das Cruzes University (2013). He had his internship in the lab and has experience in cell culture and scaffolds of carbon nanotubes from the Hospital Albert Einstein from 2012 to 2013. He received his Master's degree in Sciences from UNIFESP in 2016. His research involved the study on labeling stem cells with iron oxide nanoparticles for tracking of celullar therapy in the AVC animal model. He has experience in the use of nanomaterials and stem cell for regeneration tissues.

Helio Rodrigues da Silva
Hospital Israelita Albert Einstein, São Paulo, Brazil; and Santa Casa Misericórdia de São Paulo, São Paulo, Brazil

Helio Rodrigues da Silva received his Bachelor's degree in Biomedicine from UMESP, Brazil, in 2005 and his Doctorate Degree in Health Sciences from FCMSCSP, Brazil, in 2016. He has experience in nanotechnology and animal experimentation, with emphasis in therapeutic strategies for stroke using nanobiotechnological tools.

Leopoldo Penteado Nucci
Universidade Federal de São Paulo, Unifesp, São Paulo, Brazil; Faculdade Estácio de Sá de Goiás, Fesgo, Goiânia, Brazil

Leopoldo Penteado Nucci is a dentist, specializing in periodontology and intensive care and has a Master and PhD degrees in Science from the University of São Paulo, Brazil. He has experience in preclinical and structural neuroimaging and nanobiotechnology applied in Parkinson's disease, stroke, and brain tumor animal models. He has worked as a research collaborator in nanobiotechnology research group and dentistry in the Hospital Israelita Albert Einstein. His current research interest is in developing novel therapy methods associated with nanobiotechnology for neurodegenerative disease.

Mariana Penteado Nucci-da-Silva
LIM44, Departamento de Radiologia, USP, São Paulo, Brazil

Mariana Penteado Nucci-da-Silva graduated as a Physiotherapist from Santa Cecília University in 2000. She obtained her PhD in Science from the University of São Paulo, Brazil, in 2014, and became Scientific Researcher III of the Laboratory of Medical Investigation in Magnetic Resonance at Radiology Institute of Faculty of Medicine – University of São Paulo. She has experience in functional magnetic resonance image technique in neurologic disease, mainly hypoxic events and nanobiotechnology that can be applied in stroke and brain tumor animal models of neurologic disease, as well as animal behavior analyses and neuroimage analysis in animal models.

Lionel Fernel Gamarra
Hospital Israelita Albert Einstein, São Paulo, Brazil; Universidade Federal de São Paulo, Unifesp, São Paulo, Brazil; and Santa Casa Misericórdia de São Paulo, São Paulo, Brazil,
lgamarra@einstein.br

Lionel Fernel Gamarra obtained his Bachelor's degree in Physics from the National University Federico Villareal (1998) and his Master's degree and PhD in Physics from the University of São Paulo. He has a postdoctoral at the Hospital Israelita Albert Einstein, where he is currently the principal investigator of the Neuronanobiotechnology lab. His research group develops novel and effective nanobiotechnological tools for diagnosis and/or treatment of brain cancers or stroke using stem cells, therapeutics, nanoparticles, imaging, and/or diagnosis of neurological diseases and the effect of magnetic hyperthermia in brain cancers.